BRUSHLESS DC MOTOR CONTROL UNDER VARYING LOAD CONDITIONS

A Thesis Submitted to
The Graduate School of Engineering and Sciences of
Izmir Institute of Technology
In Partial Fulfillment of the Requirements for the Degree of

MASTER OF SCIENCE

in Electronics and Communication Engineering

by
Salih Murat KARA

December 2017
İZMİR

We approve the thesis of **Salih Murat KARA**

Examining Committee Members:

_____
Asst. Prof. Dr. Barbaros ÖZDEMİREL
Department of Electrical and Electronics Engineering
Izmir Institute of Technology

_____
Prof. Dr. Enver TATLICIOĞLU
Department of Electrical and Electronics Engineering
Izmir Institute of Technology

_____
Prof. Dr. Aydoğan SAVRAN
Department of Electrical and Electronics Engineering
Ege University

28 December 2017

_____
Asst. Prof. Dr. Barbaros ÖZDEMİREL
Supervisor, Department of Electrical and Electronics Engineering
Izmir Institute of Technology

_____	_____
Prof. Dr. Enver TATLICIOĞLU	**Prof. Dr. Aysun SOFUOĞLU**
Head of The Department of	Dean of the Graduate School of
Electrical and Electronics Engineering	Engineering and Sciences

ACKNOWLEDGEMENTS

ABSTRACT

BRUSHLESS DIRECT CURRENT MOTOR CONTROL UNDER VARYING LOAD CONDITIONS

Brushless direct current motors (BLDCMs) are popular in various applications due to their high-power density, wide speed range and control flexibility. They work without brushes and require electronic commutation, where stator's current state is synchronized with rotor position. Various methods are used to determine the rotor position. Sensorless method of position detection is preferable instead of external sensors, because external sensors are not cost effective and they create wiring complexity.

This thesis presents control methods and driver algorithms for BLDCM under variable load conditions from start-up to continuous run with speed regulation. The inductive sense method, which is one of the sensorless position measurement methods, is used when the motor is stationary and at low speed. The rotor position was accurately calculated by using this method based on inductance differences. Afterwards, back electromotive force (BEMF) sense method was used at high speed.

The drive parameters, mainly the step time and excitation step, are adjusted according to the rotor position to drive the motor efficiently. The dynamic control of the drive parameters is done by estimating the load with the rotor position.

ÖZET

DEĞİŞKEN YÜK KOŞULLARI ALTINDA
FIRÇASIZ DOĞRU AKIM MOTOR DENETİMİ

Fırçasız doğru akım motorları, yüksek güç yoğunluğu, geniş hız aralığı ve kontrol esnekliği nedeniyle çeşitli uygulamalarda yaygın kullanılır. Bu motorlar fırça olmadan çalışır ve statör alanı ile rotor pozisyonunu senkronize etmek için elektronik komütasyona ihtiyaç duyarlar. Rotor konumunu belirlemek için çeşitli yöntemler kullanılır. Harici sensörler maliyetli olduğu ve kablolama karmaşıklığı yarattığı için sensörsüz konum belirleme yöntemi tercih edilir.

Bu tezde değişken yük koşullarında fırçasız doğru akım motorların sensörsüz kalkış ve hız regülasyonu için kontrol yöntemleri ve sürücü algoritmaları sunulmuştur. Motor dururken ve düşük hızda çalışırken sensörsüz konum ölçümü yöntemlerinden biri olan indüktans algılama (inductive sense) kullanılmıştır. Bu yöntemle indüktans farkından yararlanılarak hassas bir şekilde rotor konumu hesaplanabilmiştir. Motor yüksek hızda çalışırken geri elektromotor kuvvet algılama yöntemi kullanılmıştır.

Motorun verimli bir şekilde sürülebilmesi için sürücü parametrelerinin uygun bir şekilde rotor konumuna göre ayarlanması gerektiğinden, özellikle uyartımlar arası uygulanan zaman ve uyartım yönü parametrelerini belirleyebilmek için sensörsüz konum belirleme yöntemiyle hassas bir şekilde bulunan rotor konumu ile yük tahmini yapılarak motor yüküne göre sürücü parametrelerinin dinamik kontrolü gerçekleştirilmiştir.

TABLE OF CONTENTS

LIST OF FIGURES

LIST OF TABLES

LIST OF ABBREVIATIONS

Abbreviations

AC	Alternating current
ADC	Analog to digital converter
BEMF	Back electromotive force
BLDC	Brushless direct current
BLDCM	Brushless direct current motor
CPU	Central processing unit
DC	Direct current
ISR	Interrupt service routine
LUT	Lookup table
MCU	Microcontroller unit
MOSFET	Metal-oxide-semiconductor field-effect transistor
PI	Proportional-integral
PWM	Pulse width modulation
Y	Star or wye connection
ZC	Zero cross

CHAPTER 1

INTRODUCTION

1.1. Brushless Direct Current Motors

Electric motors are common components in all kinds of applications that require electromechanical energy conversion. They have various areas of application, such as household appliances, power tools, electric vehicles, and industrial manufacturing equipment. Also, they are easy to use since electricity is accessible almost everywhere.

Electric motors are reliable and energy efficient, and their technology has been continuously improved since their invention. Development of electric motors and drivers depends on other technologies, such as microelectronics and driver algorithms. New microelectronic components and algorithms are being created continuously, and with the help of these improvements, efficiency of electric motors increases.

The motor drivers are motion control systems that consist of electronics hardware and software with algorithms. There are two important reasons for the development of driver technology (Miller 1989). First is the necessity for new technology to satisfy industry's demands, second is the need to support innovative technology, such as the BLDCMs and switch reluctance motors.

Electric motors are categorized into two types as direct current (DC) and alternating current (AC) motors depending on supplying voltage. Motors that use AC voltage have two types which are synchronous and asynchronous motors. Synchronous motors create magnetic field in rotor by using permanent magnets or electromagnets, whereas induction method is used for asynchronous motors. On the other hand, DC motors use DC supply. A conventional DC motor has brushes that commutate the current flow through the collector on the rotor. As an alternative, BLDCM is one of the synchronous machine types that has characteristics similar to brushed DC motor. After increased availability of permanent magnet materials and high voltage transistors, studies on BLDCMs have been accelerated.

When brushed and brushless DC motors are compared, the main difference between them is the brushes. When brushes commutate the motor mechanically, the

friction of brushes consumes additional energy. BLDCMs are more reliable than ordinary brushed DC motors, and they are more suitable for speed control and regulation. The other differences are summarized in Table 1.1.

Table 1.1. Comparison between brushed DC motors and BLDCM.

Brushed DC Motors	BLDCM
Maintenance problem	Maintenance free
Shorter life	Longer life
Mechanical commutator	Electronic commutator
High electrical and mechanical noise	Low electrical and mechanical noise
Simple control	Complex control
Low efficiency	High efficiency

BLDCM can be studied in three main parts which are stator, rotor, and electronic commutator. The rotor is the rotating part of the motor; its magnetic field is provided from permanent magnets generally. The stator is the stationary part of the motor; its magnetic field is produced via copper wires in slots. The electronic commutator determines the sequence of driving currents through the stator wires in BLDCM, replacing the function of brushes in conventional motors.

There are two flux directions which are axial flux and radial flux for electric motors. The radial flux motors are divided into two categories which are inrunner and outrunner rotor motors as shown in Figure 1.1.
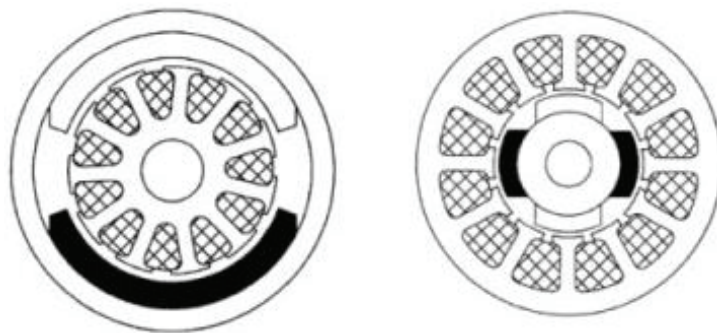
Figure 1.1. Differences between inrunner and outrunner motor.

Coils in the stator carry current, and these coils are commutated sequentially to rotate the rotor. BLDCMs can be constructed with various numbers of phases from one phase to four phase. Three phase configuration is the most common for BLDCMs. Motors with more than three phases are not common, because the number of power electronics devices for electronic commutator increases with the number of phases (Hanselman 2006).

When three-phase BLDCMs are driven, two phases in the stator carry a current that flows from positive supply to the ground, while the remaining phase is not connected to any node in six-step commutation method. Phase sequence is changed for each step to control current direction resulting in varying magnetic field in the stator. Also, permanent magnets produce a magnetic field on the rotor. The interaction between rotor and stator fields generates the torque that runs the BLDCM. In order to maintain motor efficiency, stator coils need to be commutated properly by utilizing one of the position sensing methods.

1.2. Problem Statement and Proposed work

BLDCM has several advantages such as high efficiency, high torque output to size ratio, long life, low electronic and mechanic noise, and maintenance-free usage. However, electronic commutation is needed for the stator's current state to be synchronized with rotor position. Several methods and algorithms are used in order to determine the rotor position. External sensors, such as hall-effect, optical, and mechanical sensors can be used, but they are not cost effective and they create wiring complexity. Furthermore, some applications are not suitable to work with electronic position sensors. For example, electric motor of refrigeration compressor works in oil, and oil can affect the position sensors adversely. Also there may not be enough space to place position sensors. For these reasons, the sensorless method can be preferable. The method based on measurement of BEMF (back electromotive force) is a very common approach. Unfortunately, the BEMF detection approach cannot be applied when the rotor moves at a very low speed or when it is at standstill, because BEMF cannot be measured in these conditions. Also, load changes on the motor, cause variable speed, and this variation affects the commutation approach. Therefore, a different approach called "inductive sense" is required for start-up and low speed commutation (Jang, Park,

and Chang 2002). Drive parameters are changed according to the load estimation by finding the position of the rotor more precisely. If these approaches are used together in a system, then that system can deal with problems of sensorless control in different states. The main focus of this thesis is development of a BLDCM control system to implement different control algorithms and to monitor BLDCM under varying load conditions for testing purposes.

1.3. Thesis Organization

In this thesis, sensorless control methods for BLDCMs are presented. In the second chapter, the principles of BLDCM driver design, commutation methods, rotor position detection, and BLDCM start-up studies are described. In the third chapter, controller implementation for BLDCM is explained. The controller, bridge driver, pulse width modulation, BEMF detection circuit, inductive sense position detection, and motor speed control are explained in this section. The fourth chapter explains the algorithms that are used to implement BLDCM control methods. Fifth chapter presents the performance results of the control algorithms under variable load conditions. Finally, achievements within the scope of the thesis are summarized and the possibilities for future work are explained in chapter six.

CHAPTER 2

REVIEW OF BRUSHLESS DC MOTOR DRIVERS

Electric motors convert electrical energy into mechanical energy, and it is very important to achieve as high as possible conversion efficiency for every type of motor. In this chapter, the principles of BLDCM driver design are described, and common commutation methods and positioning requirements of the rotor during the excitation steps are explained.

2.1. BLDC Motor Driver Principles

Power supply for a BLDC motor is a fixed DC source that can be obtained from rectified AC power or any battery. A rotating magnetic field is generated by controlling the stator phase currents electronically which requires continuous detection of rotor position. Electronic commutation eliminates mechanical contacts and their reliability problems. However, complexity and cost of the driver electronics are the disadvantages. With the mechanical force produced, the rotor is aligned to a specific region (alignment process). This alignment is related to the composition of the magnetic force vectors. By changing these forces periodically, a continuous torque can be obtained.

2.1.1. Alignment Process

Figure 2.1 shows a simplified model of a BLDCM which has three phase connections that are called A, B and C. The current direction in coils is indicated by arrows. The position of the rotor shown as a permanent magnet bar is controlled by the configuration of currents through three phases. The magnet aligns to position step-0 when a current is applied from A through B. The next alignment position is step-1 when a current is driven from A to C.
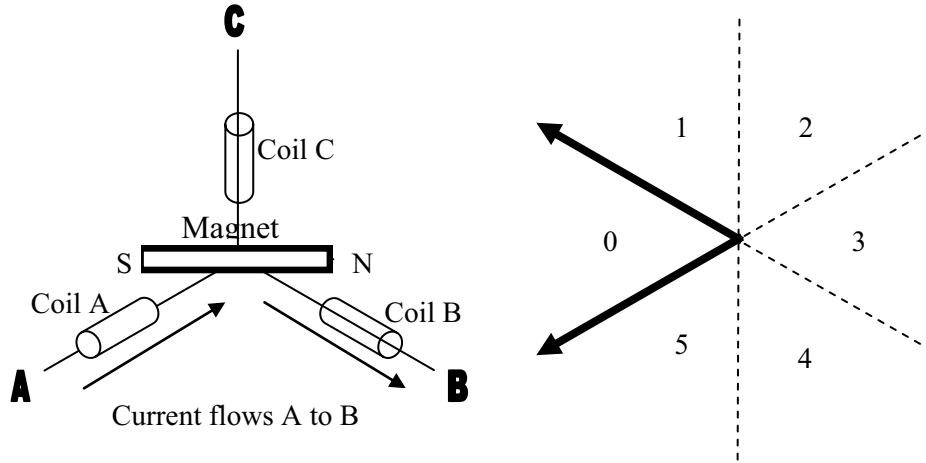
Figure 2.1. Rotor aligns at step-0 when current flows from A to B.

2.1.2. Torque and BEMF of BLDC Motor

Torque output of a BLDCM depends on direct control of the stator winding current. The torque given by DC motor equation is (Polka 2003):

$$\tau = K_a \, \Phi_t \, I_{dc} \qquad (2.1)$$

where:

τ = Torque (N.m.)

I_{dc} = Average dc bus current

Φ_t = Total flux per pole in webers

K_a = Winding constant which is equal to $P \, Nc / (2\pi)$

where:

P = Number of motor poles

Nc = total number of current-carrying conductors

Nc = 2 / 3 × Slots × Coil sides per slot × Turns per coil / Circuits

The BEMF generated by the rotor magnet can be expressed as (Lita and Cheles 2008):

$$BEMF = N \, l \, r \, B \, \omega \qquad (2.2)$$

where:

> N = Number of windings per phase
>
> l = Length of the rotor
>
> r = Internal radius of the rotor
>
> B = Rotor magnetic flux density
>
> ω = Angular velocity

The output torque of motor depends on magnetic flux and current. Stator current determines the output torque, and it can also be measured to provide torque feedback for a closed-loop system. When a BLDC motor needs reverse torque, the current can be applied in the opposite direction. The steady-state speed of a BLDC motor eventually depends on the output torque, and it is sufficient to control the average voltage applied to motor terminals in order to change the speed of the motor. For changing the stator voltage efficiently, PWM (pulse width modulation) is the most common method. Additionally, a more accurate speed control system can be obtained by adding a tachometer or a rotary encoder on the rotor. This addition increases the cost of the controller and its cable complexity.

2.2. Commutation Methods

The driving performance of the motor may vary depending on the voltage waveforms applied to the motor windings. Two commutation methods, trapezoidal and sinusoidal, are used in BLDC motor drives as follows.

2.2.1. Trapezoidal Commutation

This method is also called six-step commutation. In this method, two of the three windings are energized at the same time. The remaining winding which is left floating gives position information by using BEMF signal in sensorless control. Each one of the six-steps is equivalent to 60 electrical degree rotation. So, these six steps make one complete electrical cycle. Figure 2.2 shows BLDC motor's six-step commutation. The arrows in the Figure 2.2 show the directions of current flowing through the motor windings for each step.
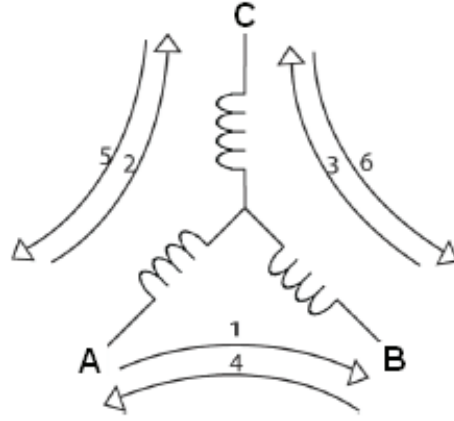
Figure 2.2. Six-steps of trapezoidal commutation.

In trapezoidal method, steps are applied properly in order to generate a rotating field in the stator. Electrical repetition frequency in the stator is proportional to the mechanical rotor speed depending on number of magnetic pole pairs on the rotor. Mechanical rotation speed is equal to the electrical frequency divided by the number of pole pairs.

Generation of torque is provided by the phase angle between the stator field and the rotor field. Maximum torque (T_{max}) is obtained when there is 90 degree phase advance between the fields. In the six-step commutation method, stator field only moves 60 electrical degrees in each step, and the rotor field follows the stator field continuously. The maximum torque zone slips in the amount of plus and minus 30 electrical degrees during a 60-degree rotation (Nilsson and Modrack 2013). In an ordinary BLDC motor, the torque has a sinusoidal variation as a function of the phase advance, and the minimum torque during a step is given by

$$T_{min} = T_{max} \left[\sin(90^\circ - 30^\circ)\right] \tag{2.3}$$

$$T_{min} = T_{max}\ 0.866 \tag{2.4}$$

Torque ripple (T_{ripple}) is given by the difference between maximum and minimum torque:

$$T_{ripple} = T_{max} - T_{min} = T_{max}\ (1 - 0866) \tag{2.5}$$

resulting in

$$\frac{T_{ripple}}{T_{max}} = 13.4 \ \%$$ (2.6)

Trapezoidal commutation method is simple because six-steps complete one electrical cycle, and the operation of gates requires simple hardware. However, it has disadvantages of speed and torque ripples.

2.2.2. Sinusoidal Commutation

In this method, all three phases of the motor are energized with sinusoidal voltages at the same time. This allows generation of smoother torque and ability of controlling the motor more precisely. In order to obtain a precise sinusoidal waveform, one degree or better resolution of position information is necessary. In addition, precise generation of a smooth torque profile also requires BEMF waveform matching.

2.3. Rotor Position Detection

The accurate detection of rotor position for BLDCMs is necessary. Any position estimation error may cause inadequate performance, and it may also result in motor failure. Rotor position can be detected by sensored or sensorless methods. In the sensored method, external components, such as hall-effect, optical, or mechanical sensors are used. These sensors are mounted on the motor and they are connected to the controller processor. On the other hand, sensorless method does not use any physical sensors, reducing hardware cost and wiring complexity.

2.3.1. Sensored Approach

The simplest and the most common technique used is the application of external sensors, however, these may increase the total cost of the motor. When external sensors are preferred for BLDCM drive, they may also increase cable complexity. Motion sensors based on magnetic field detection principles, such as hall sensors, are the most

commonly used sensor types due to their low cost and high reliability.

Hall sensor is based on hall effect theory which can be summarized as "If an electric current carrying conductor is kept in a magnetic field, the magnetic field exerts a transverse force on the moving charge carriers that tends to push them to one side of the conductor." Magnetic influence on the conductor produces a measurable voltage between the two sides of the conductor. This transverse voltage is called Hall effect which was discovered by Edvin Hall in 1879 (Hall 1879).

While brushed DC motors have mechanical commutators that consist of a collector mounted on the rotor and brushes, BLDC motors are controlled electronically. Stator windings of a BLDCM should be energized in a proper sequence. Rotor position information is necessary to follow the required sequence of the commutation steps. Most of the BLDC motors have three Hall sensors embedded into the stator at the non-driving end of the motor (Yedamale 2003).

Position of the hall sensors on the stator is critical, because controller assigns commutation steps according to the data coming from hall sensors. Any kind of detection error can cause wrong commutation execution. In order to reduce design complexity, hall sensors are mounted with additional hall sensor magnets as shown in Figure 2.3. These magnets are smaller than the magnets of the rotor and only used for position detection. Therefore, information of rotor position can be determined using hall sensors, independent of the motor structure. As a result, hall sensor magnets provide the same position information with the main magnet of the rotor with a flexible positioning option. Users can adjust the position of hall sensors to achieve the best performance.
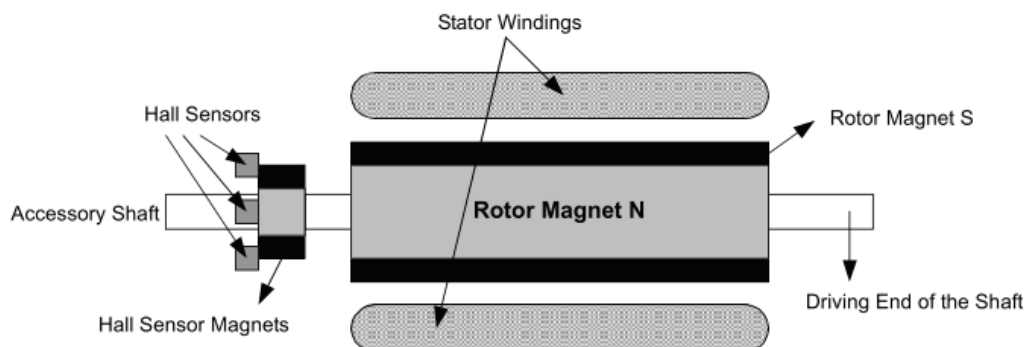
Figure 2.3. Position of hall sensors on the non-driving end of the motor
(Source: Yedamale 2003).
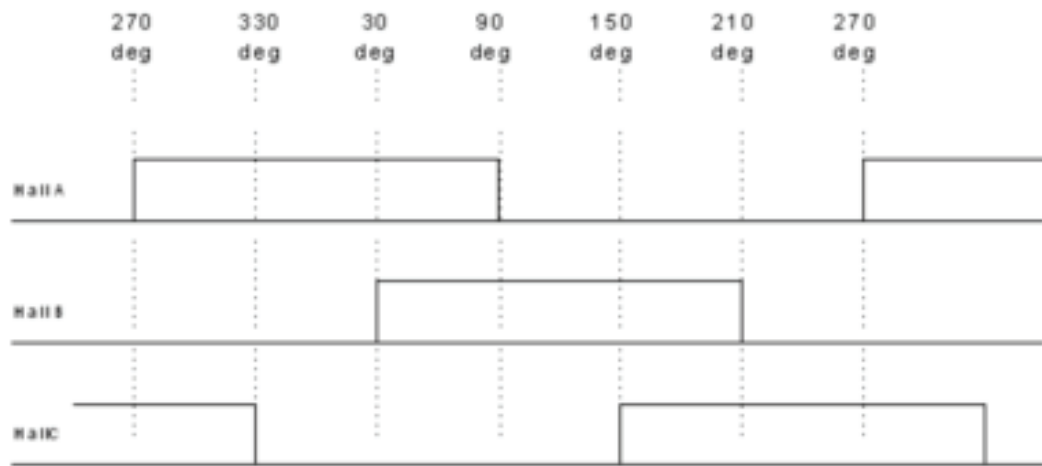
Figure 2.4. Hall sensor position information.

Hall sensor magnets affect the hall sensors, so that they deliver position information signal to the controller. The output information of Hall sensors are shown in Figure 2.4. The controller takes information from the hall sensors, processes these signals and decides where the rotor is. Then, motor phases are excited according to the rotor position.

2.3.2. Sensorless Approach

As sensored BLDCMs have durability and cost problems, this situation encouraged further research on sensorless BLDCMs. As position sensors can be fragile in some applications, sensorless approach solves the detection problem inside the motor controller with the use of voltage and current response of motor. The physical principles of BEMF sense method and inductive sense method are explained in the following sections. Several sensorless drive approaches to improve controller stability and efficiency are summarized in the last section.

2.3.2.1. BEMF Sensing Method

One of the most common sensorless control approaches is based on BEMF signal. In this method, BEMF signal induced in motor coils becomes available in each winding while BLDCM rotates. In accordance with Lenz's law (Yedamale 2003), the

sensible BEMF signal is in the reverse direction with the applied voltage. The amplitude of BEMF signal is proportional to the rotation speed. Hence, detection of BEMF signal is not possible at low speed or stand still condition. As Figure 2.5 shows, zero cross of the BEMF signal can be detected to determine exact commutation point of the motor.

Commutation step can be determined by finding zero cross point of each phase by using a comparator. When the unpowered winding signals are compared with half of the DC bus voltage, the comparator output changes indicating that the zero crossing point is detected (Gamazo-Real, Vázquez-Sánchez, and Gómez-Gil 2010). Figure 2.6 shows the basic circuitry for catching zero cross point on a winding. All zero cross points can be detected using two more comparators.
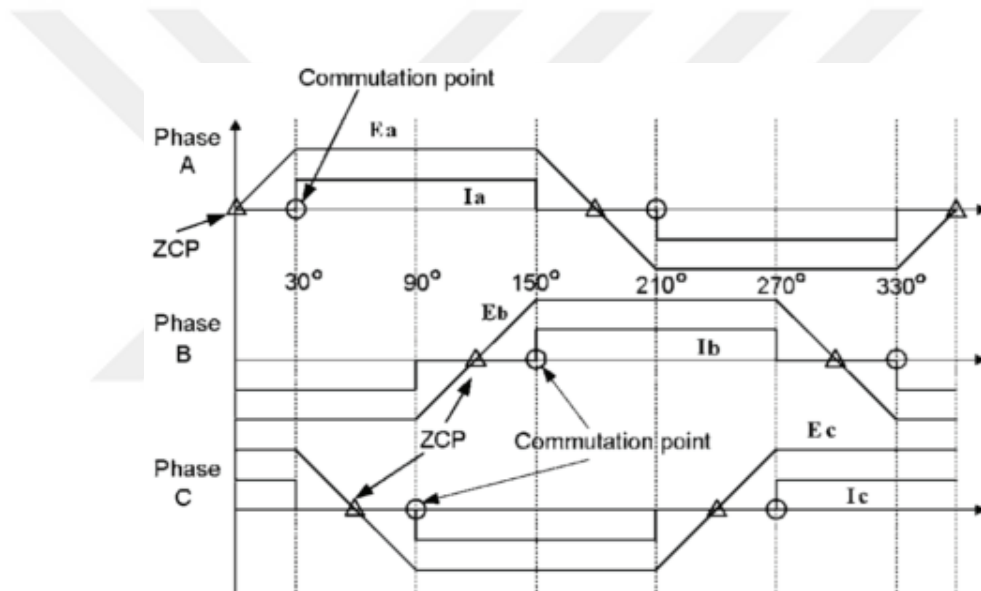
Figure 2.5. Zero cross and commutation points on BEMF signal.
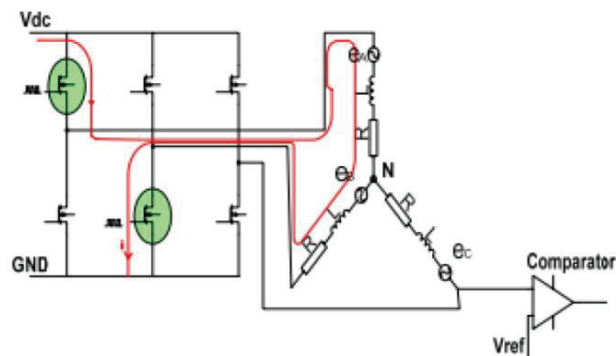
Figure 2.6. One step of current flow path.

In order to generate maximum torque, motor should be commutated every 60 electrical degree, and commutation step must be on maximum torque zone. After finding zero cross point, the microcontroller can arrange the next commutation state, and the motor runs without any physical sensors (Ikhlas 2015).

2.3.2.2. Inductive Sense Method

Inductive sense is a method of determining rotor position by measuring the effective inductance of motor windings for every commutation step without using any external sensors. This method has been used since 1990s in controllers of small BLDCMs such as, spindle drives of computer hard disks. The ferromagnetic material of BLDC motor has nonlinear magnetic saturation characteristic as shown in Figure 2.7. This is the basis for determination of the rotor position. As a result of the applied magnetic field H, the magnetic flux density B on the material is given by

$$B = \mu\, H \tag{2.7}$$

where, μ is the permeability of the ferromagnetic material.

Although the difference in applied magnetic field strength (ΔH) is the same, a different magnetic flux density may occur depending on magnetic behavior of the material. Since the magnetic permeability near the saturation region is low, this results in less magnetic flux density.
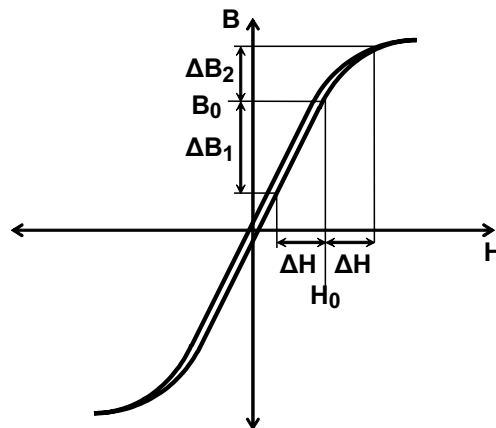
Figure 2.7. Saturation of magnetic flux density B on the hysteresis curve.

Stator's ferromagnetic material is influenced by the interaction between the rotor pole and the stator pole. When the rotor pole's magnetization direction is the same as the stator pole's magnetization direction, the material of stator reaches saturation and the inductance decreases. On the other hand, when the magnetizations are in opposite directions, the material does not reach saturation, and it remains in the linear region resulting in a higher inductance. As a result, the inductances of stator windings become a function of the rotor position (Mingyao, Zhiyao, and Keman 2008).

The voltage function across the conducting phase winding can be expressed as:

$$V_{dc} = i\, R_S + L_S \frac{di}{dt} \tag{2.8}$$

where, V_{dc} is the DC-link voltage. R_S and L_S are the equivalent resistance, and inductance of stator phase winding respectively. The phase current can be obtained as:

$$i(t) = \frac{V_{dc}}{R_S}(1 - e^{-t/\tau}) \tag{2.9}$$

where $\tau = \frac{L_S}{R_S}$ is the time constant of the stator winding.

The inductance of a coil with a ferromagnetic core varies with current, because the permeability of ferromagnetic materials changes with applied magnetic field. Figure 2.8 shows the time variation of the current when the inductances are different.
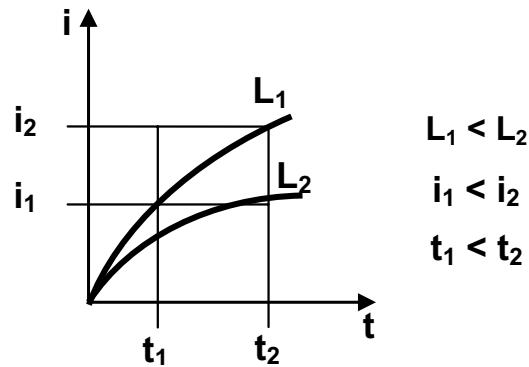
Figure 2.8. Time variation of current threshold for position detection.

Practically, the lowest inductance can be detected in two ways. As it is shown in the Figure 2.8, when inductances are different, like $L_1 < L_2$, and the fixed voltage is applied, i_2 current with inductance L_1, and i_1 current with inductance L_2 occurs after t_2. In this case, when constant time is applied, high current value shows low inductance. Another method of detection is to set a common current threshold such as i_1, so that the lower inductance reaches the threshold in a shorter time.

2.4. Sensorless BLDCM Studies

The review of literature about sensorless operation of brushless DC machines is presented in this part. Methods which are explained include:

1. Finding drive parameters based on fundamental machine equations and algebraic manipulations by using measured currents and voltages.
2. Using observers to find rotor position and speed.
3. Using BEMF detection methods to find rotor position and speed.
4. Starting techniques.

Rotor position can be estimated, if the machine parameters and the relationship of flux linkage with rotor position are known. The speed determined is related to the rate of change of the flux linkage from integration results. Line-to-line voltages may be used in the calculations, and thus no neutral motor connection is required. This is an advantage of flux calculation method (Wu and Slemon 1990). Flux calculation method with advanced control strategies, such as state observer to compute the speed feedback signal (Consoli et al. 1994) and adaptive control (Liu and Cheng 1992) can be used. In another study, d-q model of the machine is used (Matsui and Shigyo 1990). The actual d-q transformed currents and voltages and those on a hypothetical axis offset from the d-q axis were compared. In another study, detection of rotor position and speed from the stator quantities are researched. Expressions for rotor position and speed in terms of stator variables are derived and verified by comparing the computed speed and angle with experimental results (Hoque and Rahman 1994).

Rotor position and speed can also be found by using observers. Kalman filter is used as a position estimator in (Dhaouadi, Mohan, and Norum 1991), (Bado, Bolognani, and Zigliotto 1992). Kalman filtering adds refinement for estimating position and speed.

Other observer-based systems, such as non-linear, full order, disturbance, reduced-order and sliding-mode are discussed in (Johnson, Ehsani, and Guzelgunler 1999).

Finding rotor position and speed by using BEMF is a common method. BEMF signal can be detected in several ways such as terminal voltage sensing, sensing of the third harmonic of the BEMF and freewheeling diode conduction method. In the terminal voltage sensing method, switching instants of the commutations can be obtained by detecting the ZC of the BEMF after a speed dependent time delay (Iizuka et al. 1985). ZC points are detected by monitoring the BEMF when the particular phase current is zero on the unexcited phase. Low pass filters are used to eliminate higher harmonics in the terminal voltages. Since BEMF amplitude is zero at rest and proportional to rotor speed, the terminal voltage sensing is not possible at low speeds. As the speed increases, the average terminal voltage and the frequency of excitation increase. Capacitive reactance in the filters varies with the frequency of excitation and causes problems at higher speeds. With this method, a reduced speed operating range is normally used, typically around 1000-6000 rpm.

Another BEMF sensing technique is based on third harmonic of the BEMF, and it can be used in determination of the switching instants in the Y-connected 120 degree current conduction operating mode of the BLDC motor (Moreira 1996). This method is not as sensitive to phase delay as the ZC method. The reactance of the filter capacitor dominates the phase angle output of the filter more than the first harmonic in this case. In addition, greater than 2/3 stator winding pole pitch is required. Provided that this condition is satisfied, the third harmonic of the rotor flux can link the stator winding and induces a third harmonic voltage component which can be detected between the motor neutral and the negative inverter bus terminal. The third harmonic flux linkage lags the third harmonic of the phase BEMF that corresponds to the commutation instants of the BLDC motor. The third harmonic method provides wider speed range (100-6000 rpm).

Another method is freewheeling diode conduction method which uses indirect sensing of the ZC of the phase BEMF to obtain the switching instants of the BLDCM (Ogarawara and Akagi 1991). In the 120 degree conducting Y-connected BLDCM, one of the phases is always open circuited. For a short period during measurement of the BEMF, there remains phase current flowing, via a freewheeling diode. This open phase current becomes zero in the middle of the commutation interval, which corresponds to the point where BEMF of the open phase crosses zero. The biggest disadvantage of this method is the requirement of six additional isolated power supplies for the comparator

circuitry for each free-wheeling diode. This technique outperforms the previously mentioned BEMF methods at low speeds (45-2300 rpm).

BLDC operation without a rotor position sensor requires some method for starting the motor. Examples of published start-up methods are open loop starting, using known initial position, kalman filter for starting, and using machine inductance variations. Open-loop starting (Ogarawara and Akagi 1991) which is also called blind commutation starting is accomplished by providing a rotating stator field which increases gradually in magnitude and frequency. This type of system may be satisfactory in certain applications, e.g. pump and fan drives. The disadvantage of this method is that the initial rotor movement direction is not predictable. Another problem exists if the stator field rotates faster than the rotor field. This causes the rotor to oscillate, requiring the stator field to decrease in frequency to allow starting. Blind commutation can be applied to increase motor speed for known and constant load condition. Blind commutation is based on decreasing step time and increasing applied voltage. This keeps motor's output torque constant. In order to increase the motor speed, step time is reduced and applied voltage is increased, because motor speed is proportional to the generated BEMF. Applied voltage is restricted by BEMF. In order to compensate this restriction, applied voltage can be increased if output torque reduction is not desired (STMicroelectronics 2000).

Another starting method, also called "align and go," uses known initial position. A simple way of setting an initial position is to excite one phase to cause the rotor to shift and lock into a known position (Ogarawara and Akagi 1991). Another starting method which uses a kalman filter, estimates rotor position from measured voltage and currents. The machines equations of non-sinusoidal waveforms are in d-q stator reference frame. At zero speed the voltages and currents are zero and the kalman filter alone cannot provide rotor position information. By injecting a d-axis current this condition is overcome and position at standstill is obtained.

The last starting technique uses machine inductance variances. In the previous start-up studies, the rotor position before starting is unknown in sensorless BLDCMs. It is necessary to estimate the position accurately in order to commutate the motor properly. Accurate position estimation can be performed with the inductive sense, and motor driver parameters can be controlled dynamically during acceleration. In a study from Taiwan, a 12 step commutation was performed with an inductive sense to find the initial rotor position with 30 degree accuracy. After initial position detection,

commutation steps are determined by reducing the inductive sense steps to two (Chang and Tzou 2007). Another study was conducted in Taiwan, to find inductance variations over voltages while it is usually done with the help of current sensor (Lai, Shyu, and Tseng 2003). In a study conducted in China, the calculation of the position was carried out with maximum +/- 7.5 degree error (Aiguo, Lang, and Qiangbiao 2015). In South Korea, the inductance variation was used to start the motor from standstill position smoothly and the motor was driven to medium speed without any vibration or time delay compared to the conventional BEMF sense sensorless algorithm (Jang, Park, and Chang 2002).

CHAPTER 3

CONTROLLER IMPLEMENTATION

In this chapter, implementation of hardware and software used in driver design for BLDCM are described. The major design requirements are timing arrangements in the controller, inverter bridge circuit, use of PWM to regulate motor power, sensorless position detection circuits, and motor speed control method.

3.1. Controller

The controller determines commutation steps, related timing arrangements, and PWM duty cycle according to data coming from the feedback circuit. ATmega2560, an 8-bit RISC architecture microcontroller manufactured by Atmel is used for implementation of all controller algorithms in this thesis.

Stator windings are energized following a predefined sequence at certain time intervals. The sequence of commutation steps is shown in Figure 3.1. Current flows from phase A to phase B, while phase C is idle at the first commutation step. According to the direction of rotation, the following commutation steps are A-C, B-C, B-A, C-A, and C-B for forward direction, and C-B, C-A, B-A, B-C, and A-C for reverse direction.
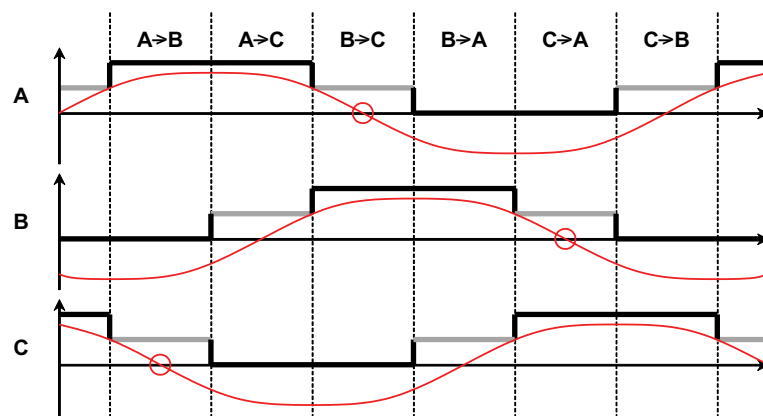
Figure 3.1. Commutation steps and BEMF waveforms; **Black high level**: driven by a PWM waveform, **Black low level:** pulled to ground, **Gray mid-level:** 3-stated during a step, **Red:** BEMF generated by 3-stated winding .

Commutation timing is determined by a 16-bit TIMER in ATmega2560. One mechanical cycle is twice as long as an electrical cycle, since four-pole motors are used. The values given in Table 3.1 and Table 3.2 show the typical timing parameters assuming that the motor speed varies between 300 rpm and 3000 rpm. In one step, timer needs to count up to 200 ms at 300 rpm, and at 3000 rpm, a 20 ms count is required.

Table 3.1. Sample timing parameters for a 4-pole BLDCM.

Sample timing parameters for a 4-pole BLDC:			
Motor speed (rpm)	**300**	**600**	**3000**
Revolutions per second (1/s)	**5**	**10**	**50**
Mechanical cycle time (ms)	**200**	**100**	**20**
Electrical cycle time (ms)	**100**	**50**	**10**
Commutation step duration (ms)	**16.7**	**8.33**	**1.67**

Table 3.2. ATmega2560 16-bit timer clock prescaler options.

ATmega2560 16-bit timer clock prescaler options:			
Prescaler	1/1	1/8	**1/64**	1/256
Frequency (MHz)	16	2	**0.25**	0.0625
Clock period (us)	0.0625	0.5	**4.0**	16
16-bit count time (ms)	4.1	32.8	**262**	1049

Timer clock frequency setting must support the time measurements at the lowest speed, since changing timer settings during operation is inconvenient. The maximum time duration that can be stored as a 16-bit integer is 262 ms when the clock frequency is 250 kHz. +/-1 rpm speed variation around 3000 rpm results in 6.66 μs variation in mechanical cycle time. +/-4 μs quantization error in time measurements corresponds to 4/6.66=0.6 rpm speed error when the target speed is 3000 rpm.

3.2. Bridge Driver

A three phase half bridge inverter is used to arrange current direction of the stator windings in the BLDC motors. The required trapezoidal waveforms are generated at the inverter output phases by using six N-channel MOSFET switches. The two MOSFETs on an half bridge should not be turned on together at any time, otherwise, this may damage the bridge and the source generator as shown in Figure 3.2. In order to avoid a short circuit, the MOSFET driver has a protection mechanism to assure that the same half bridge switches are always in opposite state.
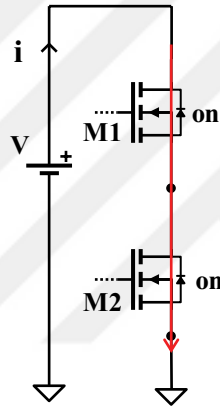
Figure 3.2. Short circuit situation on a half bridge.

Figure 3.3 shows the current flow between the supply and the ground through the motor windings. During the ON cycle of PWM, M1 and M4 MOSFETs are turned ON, and the current $i_{PS} = i_L = i_G$ flows from power supply to ground through the inductive load.

Power MOSFETs have body diodes which conduct reverse currents for recirculation. Also, power MOSFETs made with DMOS (Double-Diffused MOS) technology support reverse drain currents when the MOSFET is turned on.
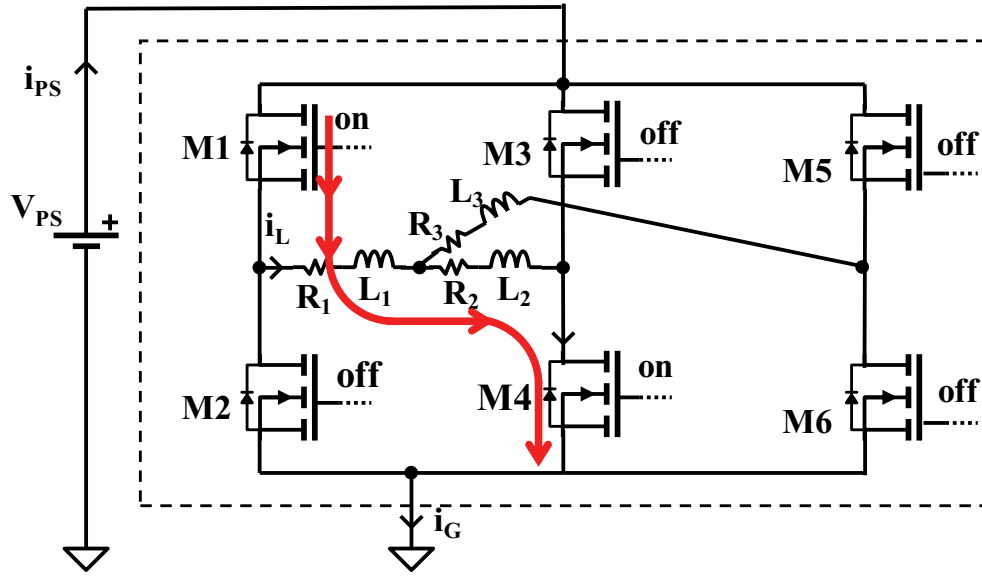
Figure 3.3. PWM ON cycle of the three phase bridge driver.

There is a large power dissipation for a short time while the MOSFET is turning ON or OFF, since both MOSFET voltage and current are not zero during switching. MOSFET switching time is specified as rise time (T_r) and fall time (T_f). There is a compromise between drain to source ON resistance, R_{DSon} and T_r, T_f of the MOSFETs which have similar power ratings. If a MOSFET with smaller R_{DSon} is chosen, then T_r and T_f are longer. Power dissipation is low when the MOSFET is ON, but it is higher when the MOSFET is switching. Also, a MOSFET with smaller R_{DSon} has bigger gate charge (Q_g) and input capacitance (C_{iss}). Powerful MOSFET drivers are required to obtain short switching times on the MOSFETs with big Q_g and C_{iss}. A high PWM frequency is required to obtain low ripple current through the load. In that case, faster switching of MOSFETs is critical to reduce power dissipation.

Determination of MOSFET type depends on the application which is being worked on. The motor driver used in this work supports motor supply voltages between 12-24 V, and the maximum required continuous current of 12 A. The selected transistor, IRLZ44N, supports 49 A continuous drain current when gate voltage is 10 V, and the maximum drain-to-source voltage is 55 V. Static R_{DSon} is 17.5 mΩ when the gate voltage is 10V. Low on-resistance, and fast switching properties make this transistor suitable for motor drive applications, since these properties decrease the power dissipation.

The HIP4086 three phase MOSFET driver manufactured by Intersil is used in this project in order to protect the inverter switches from short circuit and to drive the MOSFETs efficiently. Inside the driver, protection of switches is provided by using delayed operation and opposite logic for the high side of the three half bridges. For example, while the high side driver of the first half bridge is at logic "1", the low side driver is always at "0". HIP4086 MOSFET driver has 7 V to 15 V supply voltage range which is sufficient to drive IRFZ44N efficiently. HIP4086 control inputs are compatible with 5 V to 15 V logic levels, and it also has internal under voltage set points. It supports maximum 100 kHz switching rate which is appropriate for motor drive PWM applications. Figure 3.4 shows the basic implementation of the bridge driver circuit. Driver output states are given in Table 3.3 according to the applied input signals.
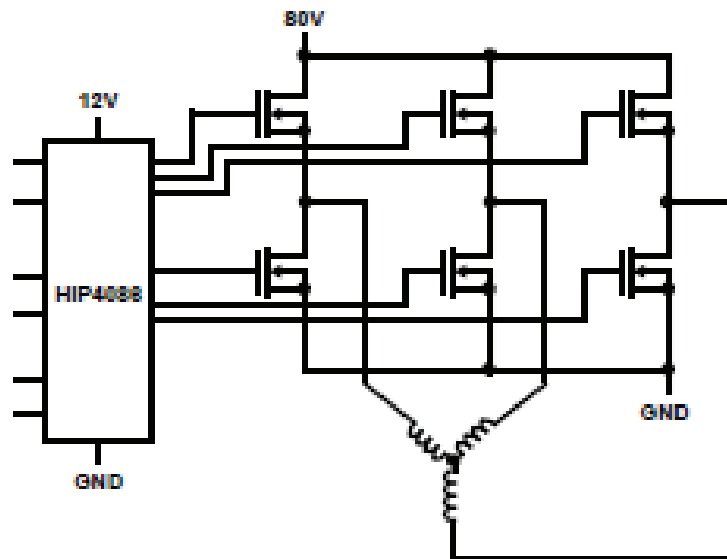
Figure 3.4. Block diagram of MOSFET Driver (Source: Harris Semiconductor 1996).

Table 3.3. MOSFET Driver truth table (Source: Harris Semiconductor 1996).

INPUT					OUTPUT	
ALI, BLI, CLI	$\overline{AHI}$, $\overline{BHI}$, $\overline{CHI}$	UV	DIS	RDEL	ALO, BLO, CLO	AHO, BHO, CHO
X	X	X	1	X	0	0
X	X	1	X	X	0	0
1	X	0	0	>100mV	1	0
0	0	0	0	X	0	1
0	1	0	0	X	0	0
1	0	0	0	<100mV	1	1

23

It is very important that the MOSFETs are controlled via a single I/O port on the microcontroller, because this allows controlling state of all gates simultaneously in a single operation. It is seen that PORTL of ATmega2560 is a suitable port that has all three PWM outputs generated by a single timer. MOSFET driver connections on PORTL of the controller are designed as shown in Table 3.4.

Table 3.4. MOSFET driver connections on PORTL.

PL3=OC5A=>nCHI	PL4=OC5B=>nBHI	PL5=OC5C=>nAHI.
PL0 => CLI	PL1 =>BLI	PL2 => ALI

Constant definitions are utilized for each phase to minimize programming complexity. Three half bridges are controlled by PORTL according to their state. For example, CVCC code is used to turn ON the high side MOSFET connected to phase C, and CGND is used to pull phase C to ground.

Table 3.5. Constant code definitions for PORTL.

```
#define  CVCC  0b00110000  // PORTL setting to pull phase C to VCC
#define  BVCC  0b00101000  // PORTL setting to pull phase B to VCC
#define  AVCC  0b00011000  // PORTL setting to pull phase A to VCC
#define  CGND  0b00000001  // PORTL setting to pull phase C to GND
#define  BGND  0b00000010  // PORTL setting to pull phase B to GND
#define  AGND  0b00000100  // PORTL setting to pull phase A to GND
#define  C3st  0b00001000  // PORTL setting to 3-state phase C
#define  B3st  0b00010000  // PORTL setting to 3-state phase B
#define  A3st  0b00100000  // PORTL setting to 3-state phase A
```

PORTL register settings for all six commutation steps are stored in an array as shown below for easy access during execution of controller tasks.

```
unsigned char ComPORTL[6] = { AVCC | BGND | C3st, // A>>B
                              AVCC | CGND | B3st, // A>>C
                              BVCC | CGND | A3st, // B>>C
                              BVCC | AGND | C3st, // B>>A
                              CVCC | AGND | B3st, // C>>A
                              CVCC | BGND | A3st  // C>>B
                          };
```

3.3. Pulse Width Modulation

Pulse Width Modulation (PWM) changes current by applying switching voltages on motor windings. The average current depending on effective voltage on stator windings determines the torque, and consequently, the speed of the motor. PWM is an efficient and convenient way of controlling current through an inductive load, and it allows flexibility for selection of the DC power supply voltage. The main parameter is PWM frequency that depends on motor specifications which are stator inductance and resistance. PWM frequency affects driver performance in two ways:

1. If PWM frequency is too low, then it causes big current ripple, and consequently, big torque ripple.

2. If PWM frequency is too high, then power efficiency of the driver decreases since driver transistors dissipate significant power every time they switch between ON and OFF states.

The following calculations of average current and ripple current show the importance of PWM frequency selection, where the average current I_{DC}, and the ripple current I_{rpl} are functions of R, L, V_p, and duty cycle as shown in Figure 3.5. The inductor current during T_{on} is given by

$$i_L(t) = \frac{V_P}{R} - (\frac{V_P}{R} - I_1)e^{-t/\tau} \tag{3.1}$$
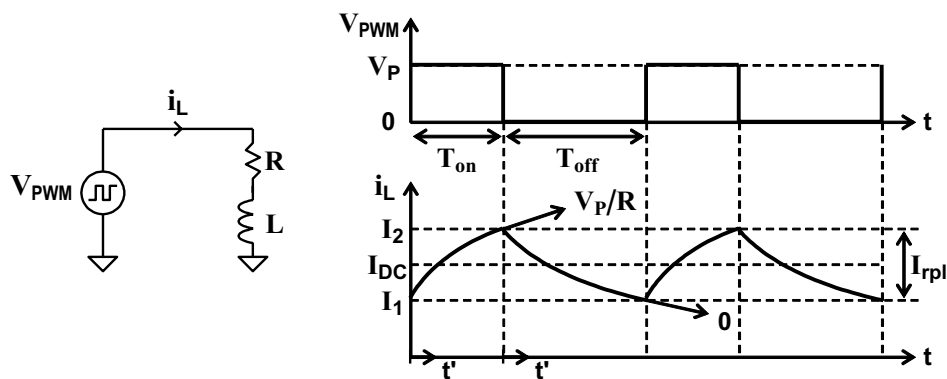
Figure 3.5. PWM signal on a basic RL circuit.

Then the peak current at the end of T_{on}:

$$I_2 = \frac{V_P}{R} - (\frac{V_P}{R} - I_1))e^{-T_{on}/\tau} \qquad (3.2)$$

Similarly, the inductor current during T_{off} is given by

$$i_L(t) = I_2\, e^{-t/\tau} \qquad (3.3)$$

At the end of T_{off} :

$$I_1 = I_2\, e^{-T_{off}/\tau} \qquad (3.4)$$

The following approximation can be used since the PWM frequency should be high enough to keep the ripple current at a reasonable level always.

$$T_{on}, T_{off} \ll \tau = \frac{L}{R} => e^{-t/\tau} \sim 1 - \frac{t}{\tau} \qquad (3.5)$$

Replacing exponential terms with the linear approximations gives

$$I_2 = I_1 + (\frac{V_P}{R} - I_1)\frac{T_{on}}{\tau} \qquad (3.6)$$

$$I_1 = I_2(1 - \frac{T_{off}}{\tau}) \qquad (3.7)$$

Then I_1 and I_2 can be calculated as

$$I_2 = \frac{\tau^2\, V_P\, \frac{T_{on}}{L}}{(T_{on} + T_{off})\tau - T_{on}\, T_{off}} \qquad (3.8)$$

$$I_1 = \frac{(1 - \frac{T_{off}}{\tau})\tau^2 V_P\, \frac{T_{on}}{L}}{(T_{on} + T_{off})\tau - T_{on}\, T_{off}} \qquad (3.9)$$

Finding average, DC current:

$$I_{DC} = \frac{I_1 + I_2}{2} = \frac{T_{on}(\tau - \frac{T_{off}}{2})\frac{V_P}{L}}{(T_{on} + T_{off}) - \frac{T_{on} T_{off}}{\tau}} \qquad (3.10)$$

$$\tau \gg T_{on} + T_{off} \implies$$

$$I_{DC} = \frac{V_P}{R}\frac{T_{on}}{T_{on} + T_{off}} = \frac{V_P}{R} \text{ x \% duty} - \text{cycle x } 100 \qquad (3.11)$$

Finding peak-to-peak ripple current:

$$I_{rpl} = I_2 - I_1 = \frac{T_{on}T_{off}\tau\frac{V_P}{L}}{(T_{on} + T_{off})\tau - T_{on} T_{off}}$$

$$\tau \gg T_{on} + T_{off} \implies I_{rpl} = \frac{T_{on} T_{off}}{T_{on}+T_{off}}\frac{V_P}{L} \qquad (3.12)$$

Maximum ripple current is obtained at 50 % duty cycle. The ratio between ripple and average currents at 50 % duty cycle:

$$\frac{I_{rpl}}{I_{DC}} = \frac{T_{on} + T_{off}}{2\tau} = \frac{1}{2 F_{pwm} \tau} \qquad (3.13)$$

3.4. BEMF Detection

BEMF signal amplitude is directly proportional to the motor speed. If the produced BEMF signal and the applied driver voltage level is higher than the sensor circuit input voltage range, then they may cause damage to the circuit. Therefore, a voltage divider should be used to protect the detection circuit. In order to determine the voltage divider ratio, BEMF voltage and supply voltage must be considered.

$$V_{BEMF} = KE \text{ [V/rpm] } Sp \text{ [rpm]} \qquad (3.14)$$

where, KE is the BEMF constant specified for the motor and Sp is the motor speed (Atmel AVR928 2013). In this setup, the divided BEMF voltage is compared with the

center-tap voltage by using differential amplifiers, and the acceptable input voltage range is 0 V-5 V. Zero crosses are obtained by taking the center tap as reference of the BEMF signal from three stated terminal. In case a center tap connection is not available on the motor, a virtual neutral can be obtained with three star connected resistors.

Three differential amplifiers and three comparators were used as shown below in Figure 3.6, in order to sense BEMF signal from 3 phases. The operational amplifiers are MCP601 manufactured by Microchip, and the comparators are LM393 by Texas Instruments. Outputs of comparators were connected to PORTD pins 0, 1 and 2.
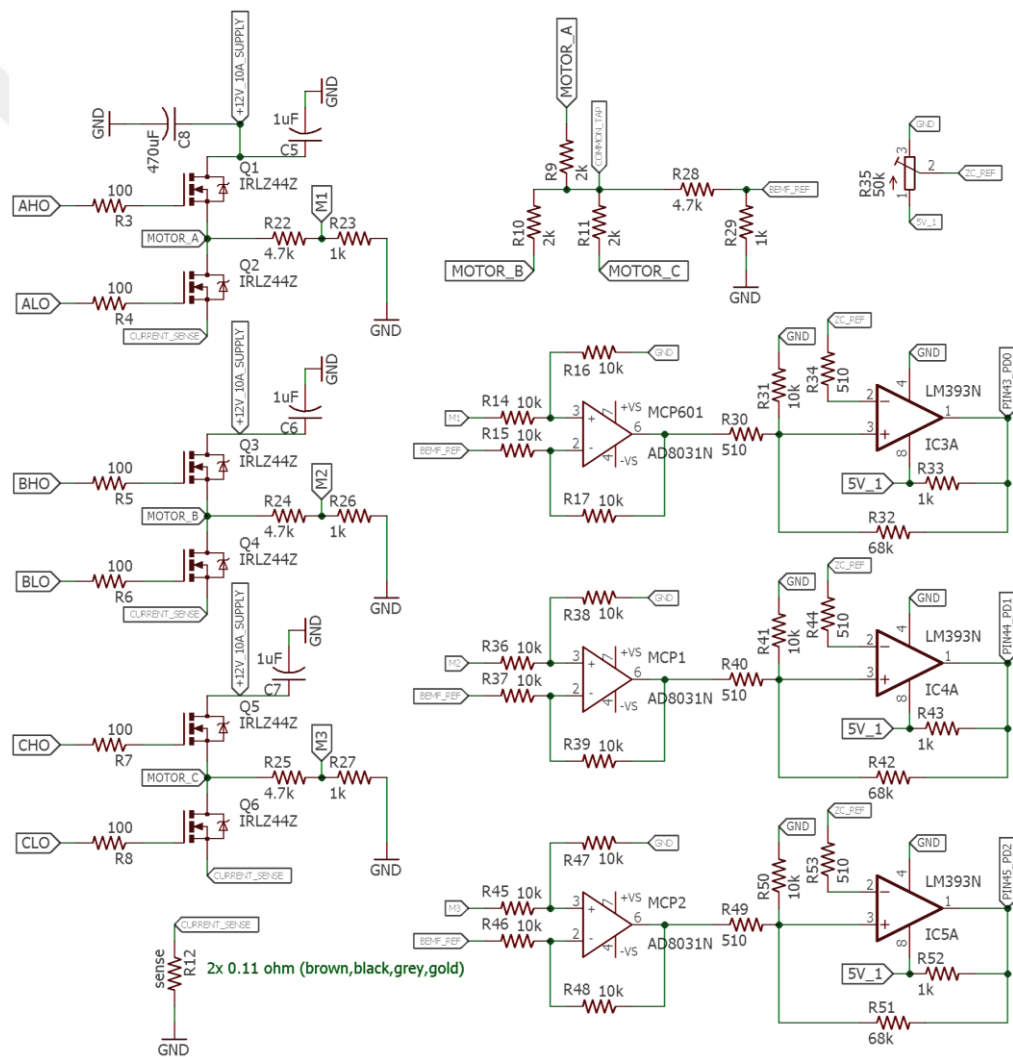
Figure 3.6. BEMF detection circuit.

3.5. Inductive Sense Current Threshold

The position of the rotor is detected at the stand still position according to the rise time of stator winding currents in the inductive sense method. The rotor magnet affects stator windings, and inductance variation becomes a function of rotor position. Six commutation steps are excited separately until the previously determined current limit threshold is reached. Figure 3.7 shows the inductive sense circuit that is composed of a comparator.
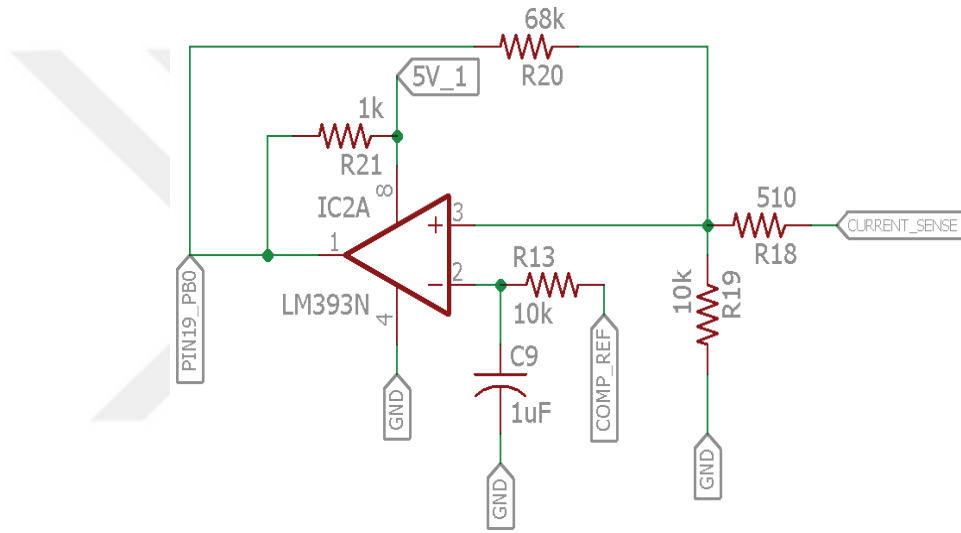
Figure 3.7. Inductive sense circuit.

The comparator compares the voltage on current sense resistor and the adjustable threshold voltage which is critical for accurate position detection. The threshold voltage must be high enough to detect the differences between six rising times and it must be kept below the current limits of the driver and the motor. The expected current response of a motor winding is given below.

$$i(t) = I (1 - \exp(-t/\tau)) \tag{3.15}$$

where, I is the steady state current τ is the time constant. Time constant τ is read when $t/\tau=1$ or when $(1 - \exp(-t/\tau)) = 0.63$. The time constant is given by L/R where, L is the

winding inductance affected by rotor location and R is the total resistance of the winding and the driver circuit.

The current threshold value is determined according to the time constants obtained at different rotor positions. To observe inductance variation according to rotor position, step-0 (current flows from phase A to phase B) is applied on the stator when rotor position is 0 and 180 electrical degrees. Current variations given in Figure 3.8 indicate that the time constants are 860 μs and 1170 μs in two cases when the same commutation step is applied. Time constant difference between two implementations shows inductance variation as a function of rotor position.
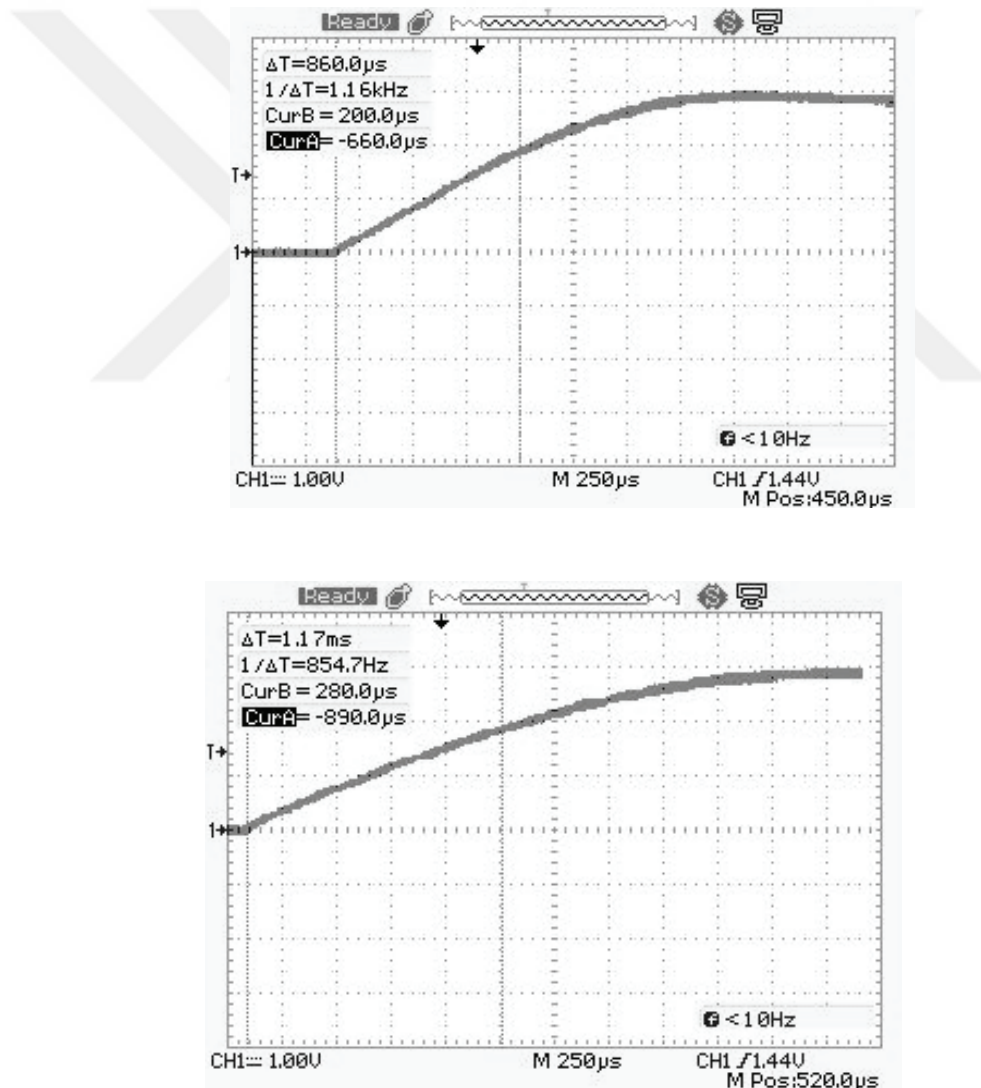
Figure 3.8. Oscilloscope captures of the inductive sense current waveforms; Top: rotor is aligned with the excitation step, Bottom: rotor position is opposite to the applied step.

Two more experimental results given in Figure 3.9 show that, low inductance zone is seen when applied step and aligned position are the same. The first plot is obtained at a fixed step, which is step-0 on the stator, when rotor position changes from 0 to 300 degrees. The second plot is obtained when different steps are applied and the rotor position is at 0 electrical degrees. Consequently, the time constant is considered as a good point to determine the threshold to obtain sufficient inductance variation for position detection.
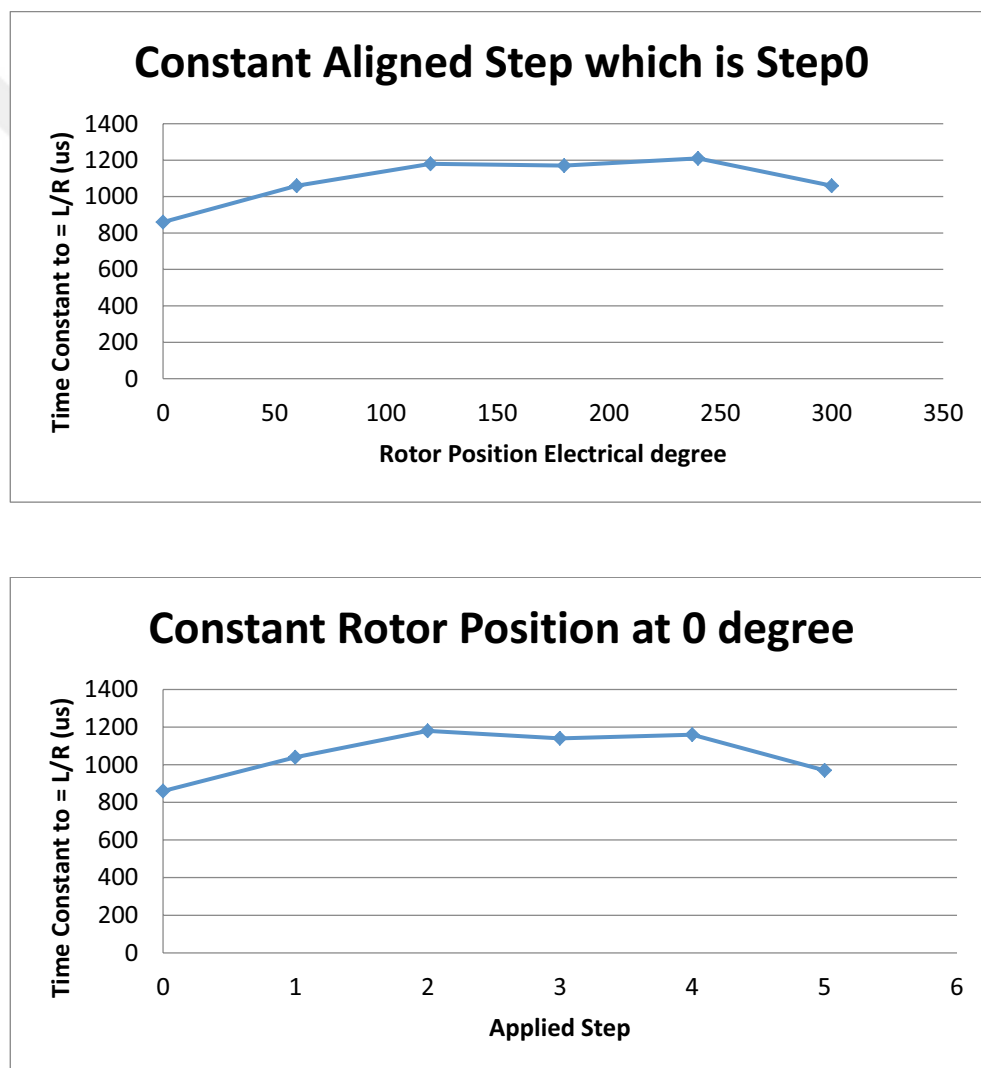
Figure 3.9. Time Constant tests.

3.6. Motor Speed Control

A proportional-integral (PI) controller determines the duty cycle of PWM according to the target speed setting and the measured ZC period. A new duty cycle is calculated periodically according to the error in the measured speed:

$$Err(t) = Spd_{set} - Spd_{mtr}(t) \tag{3.16}$$

PI controller output is given by

$$F_{out}(t) = G_p\, Err(t) + G_i \int_{t'=0}^{t} Err(t')\, dt' \tag{3.17}$$

where G_p and G_i are proportional and integral gain coefficients. Discrete domain representation of the PI controller can be obtained by using an accumulator replacing the integration in the continuous domain response:

$$Acc(k) = Acc(k-1) + Err(k) \tag{3.18}$$

$$Fout(k) = K_p\, Err(k) + K_i\, Acc(k) \tag{3.19}$$

The discrete domain gain factors are given by,

$$K_p = G_p, \text{ and } K_i = G_i\, \Delta t \tag{3.20}$$

where, Δt is the sampling time interval. The calculation of the PI controller response can be simplified by writing,

$$Fout(k) - Fout(k-1) = K_p\, [Err(k) - Err(k-1)] + K_i\, [Acc(k) - Acc(k-1)] \tag{3.21}$$

The PI controller output can be calculated based on the output value obtained in the previous sampling interval. The accumulator block can be eliminated simply by replacing the term, $[Acc(k) - Acc(k-1)]$, with $Err(k)$:

$$Fout(k) = Fout(k-1) + (K_p + K_i)\, Err(k) - K_p\, Err(k-1) \tag{3.22}$$

In motor control phase, the error term is obtained by comparing the measured mechanical or electrical cycle time with the reference cycle time corresponding to the target speed setting. The resultant timing error is a nonlinear function of motor speed, but it simplifies calculations, and it can be considered as an inverse linear function for small errors near the target speed. Duty cycle setting is obtained by scaling the PI controller output (i.e. $DCout = Fout/2^{16}$) to obtain a better adjustment range for Kp and Ki. Overflow conditions in integer arithmetic operations should be eliminated by using 32-bit long integer variables. Long process times to perform division by 2^{16} can be avoided by defining a union.

As a result, the speed control of the motor was provided during continuous operation using PI control, and motor was tested to find suitable gain factors for the controller.

CHAPTER 4

SENSORLESS COMMUTATION ALGORITHMS

BLDCM control algorithms are described in three main parts, namely start-up, synchronization and synchronous operation algorithms. The work plan of BLDCM from start up to synchronous run, and difficulties encountered during this study are explained in this chapter.

4.1. Description of Motor Start-up Sequence

The following list describes four major stages in startup process of sensorless BLDCM.

1. **Inductive sense:** It determines the initial rotor position, while motor is motionless.

2. **Start-up commutation:** Commutation steps are applied to accelerate rotor until generated BEMF becomes high enough to allow detection of zero cross (ZC) points with reasonable accuracy.

3. **Driver synchronization:** After the blind commutation, two successive BEMF ZC points are detected to determine the rotor position and speed. Then, the driver commutation steps are synchronized with the rotor motion according to the timing of these two ZC points.

4. **Synchronous commutation:** By detecting BEMF ZCs periodically, the commutation sequence is repeated while updating driver timing according to rotor position and speed. The PWM duty cycle is controlled to keep the motor speed as close as possible to the target speed determined by the user.

4.2. Implementation of Inductive Sense Position Detection

When the rotor aligns with one of the commutation steps, the magnetic flux generated by the stator windings is mostly in the same direction with the magnetization of the permanent magnet in the rotor. Any current applied to commutation step, affects magnetization in the stator and the rotor. At the saturation region small magnetic flux

changes are observed, whereas at linear region higher magnetic flux differences are observed. This results in different inductances at those regions, and inductive sense algorithm is used to determine the differences by measuring rise time of current through the motor windings for all commutation steps. By measuring the rise time, the shortest rise time of the current is obtained at the commutation step that is aligned with the rotor magnetization.

Inductive sense is implemented by exciting six commutation steps sequentially. In each step, the voltage is applied until current reaches the threshold configured according to motor inductance as shown in Figure 4.1. At the threshold, the step being executed stops and the next sequence step is excited. The timer of microcontroller measures the time until the current threshold is reached. The measured time varies for each step as a function of inductance in the motor windings. Finding shortest time among the measured rise times gives the minimum inductance (Texas Instruments 2017). Therefore, the minimum inductance represents the alignment of the current motor step. The estimated rise time appearance is shown in Figure 4.1, where the shortest time is found at step-1 which implies 60 electrical degree position.
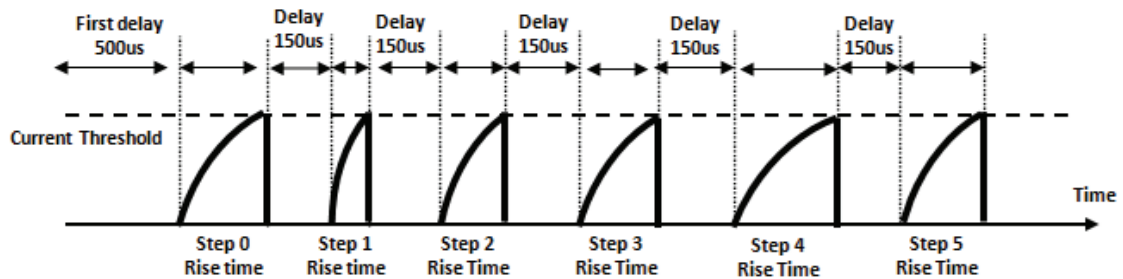
Figure 4.1. Inductive sense expected result.

The 16-bit timer-1 of ATmega2560 is used for rise time measurement with 16 MHz clock frequency providing 4.095 ms maximum count duration and 0.0625 us resolution. Timer-3 (16-bit) is used as a PWM generator to set the current threshold for inductive sense comparator with a low pass filter. The inductive sense algorithm is summarized in the following.

```
1. Setup related special function registers
2. Disable timer PWM operation, only PORTL controls commutation
3. Repeat for 6 commutation steps:
```

3.1. Wait for a settling time to avoid distortion between commutation steps
3.2. Clear Timer-1 to start measurement
3.3. Apply a commutation step until current reaches threshold.
3.4. If threshold is reached, then rise time is saved in Timer-1. If not, an error message is given after exceeding maximum allowable rise time.
3.5. 3-state all driver outputs
4. Find the step of minimum rise time

The results obtained by applying inductive sense algorithm are presented in Figure 4.2. As seen in the results, the second rise time is the smallest because the rotor is positioned at 60 electrical degrees. CH2 probe shows the current sense voltage, and CH1 probe shows the measured time.

After finding the shortest rise time step, the stored rise time measurements are used to determine the rotor position with better precision. If accurate inductive sense results are obtained as shown in Figure 4.3, a more precise angular position can be found by looking at the previous and next rise time measurements around the shortest rise time. The code given below represents a simple empirical formula to calculate the angular position in degrees.

```
dTbefore = Trise[Stepmin - 1] - Trise[Stepmin];
dTafter = Trise[Stepmin + 1] - Trise[Stepmin];
electrical_degree = (60 * Stepmin) + ( 30 * (dTbefore - dTafter)
                                     / (dTbefore + dTafter) );
```
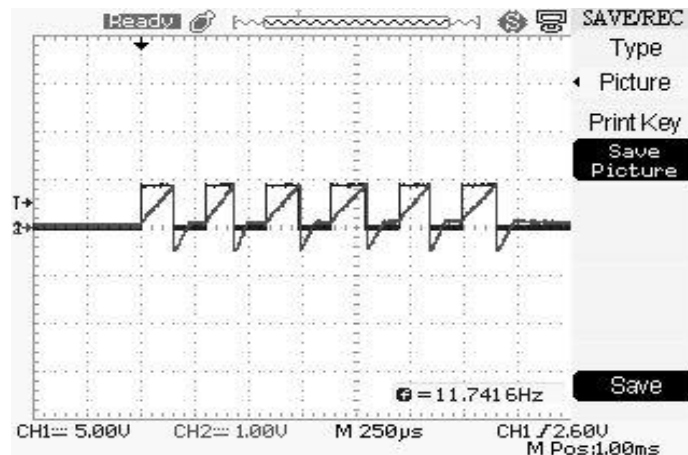

Figure 4.2. Experimental inductive sense results.
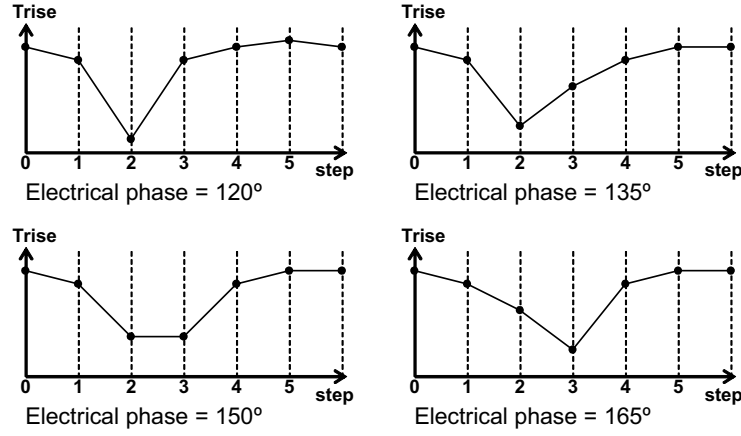
Figure 4.3. Rise time changes.

4.3. Implementation of Start-up Algorithms

In sensorless approach, blind commutation is used with the aid of inductive sense during start up. If the load torque is known and constant, then the durations of the commutation steps are calculated based on rotor inertia and load. Ideally, a constant acceleration profile is obtained by increasing motor speed linearly in time. The commutation step times are reduced following an inverse function of time as the motor speed increases. Otherwise, if the load torque is unknown, then the motor load can be estimated by repeating inductive sense between the commutation steps..

4.3.1. Blind Commutation Start-up

Blind commutation method, also called ramp-up method, is used for accelerating the motor without knowing the rotor position. Blind commutation step durations are calculated by assuming a constant acceleration profile that results in 60 electrical degree rotation in every step. The angular speed required for BEMF detection can be achieved after fifty or fewer blind commutation steps on almost all types of common BLDC motors. A look-up table for blind commutation step durations is prepared to avoid long floating point arithmetic operations that consume significant processing time in the microcontroller.

If the target constant angular acceleration is α, then the angular motion $\Delta\theta_k$ in the k'th commutation step is

$$\Delta\theta_k = 60° = \omega_k T_{LUT}[k] + \frac{\alpha}{2} T_{LUT}^2[k] \qquad (4.1)$$

where, $T_{LUT}[k]$ is the duration of k'th excitation step, and ω_k is the angular velocity right before the k'th step. The rotor is at stand still condition before the blind commutation is applied, therefore ω_0 is 0. The total angular motion θ_{sum} before the k'th step is related to the total elapsed time given by:

$$T_{sum} = \sum_{i=1}^{k-1} T_{LUT}[i] \qquad (4.2)$$

$$\theta_{sum} = (k-1)60° = \frac{\alpha}{2} T_{sum}^2 \qquad (4.3)$$

which allows calculation of T_{sum} as a function of k and α:

$$T_{sum} = \sqrt{\frac{2(k-1)60°}{\alpha}} . \qquad (4.4)$$

Angular velocity right before the k'th step is

$$\omega_k = \alpha T_{sum} = \alpha \sqrt{\frac{2(k-1)60°}{\alpha}} = \sqrt{2\alpha(k-1)60°} . \qquad (4.5)$$

$T_{LUT}[k]$ is obtained by solving:

$$60° = \omega_k T_{LUT}[k] + \frac{\alpha}{2} T_{LUT}^2[k] = \sqrt{2\alpha(k-1)60°}\, T_{LUT}[k] + \frac{\alpha}{2} T_{LUT}^2[k] \qquad (4.6)$$

$$T_{LUT}[k] = \sqrt{\frac{2\,60°}{\alpha}} \left(\sqrt{k} - \sqrt{k-1}\right) \qquad (4.7)$$

The look-up table is prepared as an array of 16-bit numbers and it is stored as part of the microcontroller code. If the target acceleration α is changed for any reason,

then the required step durations can be obtained simply by multiplying the look-up table with a scaling factor given by square root of $1/\alpha$.

Figure 4.4 shows step times and the count limits for a timer with 250 kHz clock (unit = 4 us) starting with 256 ms first step. The step durations for other acceleration rates can be obtained by a simple scaling of these step durations.

If the first step duration is 100 ms, then by multiplying the table elements by 100 and dividing the result by 256 (removing the least significant byte) the timer count for each step is obtained. Declaration of a union saves significant CPU time to apply division by 256. Long integer division operations or long integer right shift operations (i.e. >> 8) require much longer CPU time without the union declaration.

The motor speed is expected to be 50 rpm after the first step for a 4-pole motor with 100 ms first step duration. If the last step duration is determined as 8 ms, then the blind commutation ends after the motor reaches 625 rpm at the 39th step.

Blind commutation is stopped after step 4 (C>A), right before the step where a falling ZC is expected at the BEMF signal from C winding of the motor. Stopping after step 4, allows detection of two ZCs in the shortest time and reduces speed loss during synchronization. If the motor is expected to reach ~600 rpm at the end of the blind commutation, then the last step should be step 4 with duration less than 8 ms.
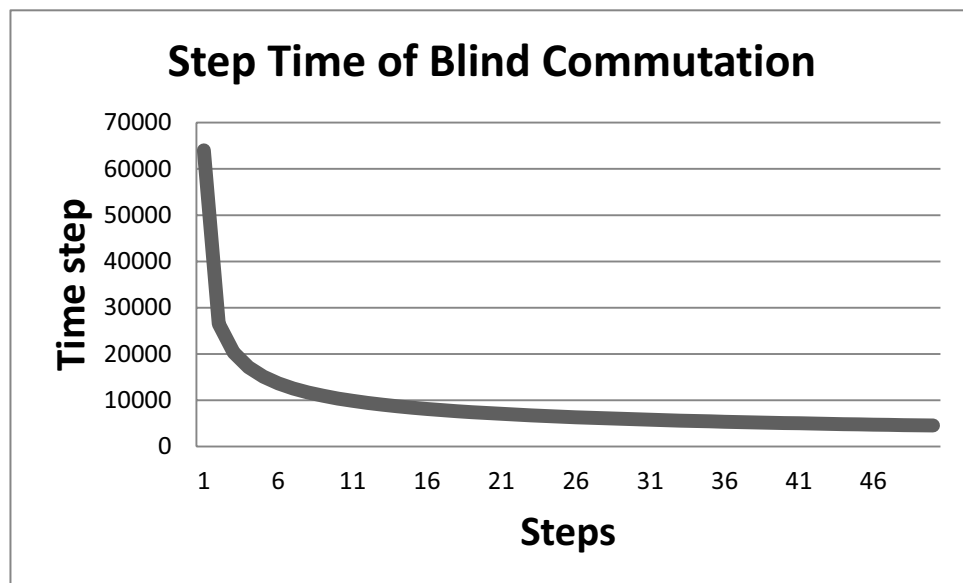

Figure 4.4. Ramp-up commutation step durations.

4.3.2. Inductive Sense Followed by Blind Commutation Acceleration

Inductive sense method can find an initial position to prevent back rotation for the first step. This method is considered for motor start-up with known load torque where the first step is determined according to the current rotor position. Finding initial position assures the rotation in forward direction during blind commutation.

After finding initial position with inductive sense, blind commutation starts at the step 90 electrical degrees ahead of the initial rotor position to obtain the maximum torque. If the rotor position does not align exactly, first excitation step should be selected as shown in Table 4.1.

Table 4.1. Relationship between step and electrical angle.

If the position data generated by inductive sense is as follows;						
Aligned step	0=A>B	1=A>C	2=B>C	3=B>A	4=C>A	5=C>B
Epos0 (ºE)	0	60	120	180	240	300
Then the first commutation step should be;						
Epos0 (ºE)	0-59	60-119	120-179	180-239	240-299	300-359
First ComStep	2=B>C	3=B>A	4=C>A	5=C>B	0=A>B	1=A>C

Blind commutation repeats six commutation steps while step durations decrease as the rotor accelerates. The first commutation step can be any of the six commutation steps, and it should be two steps ahead of the initial rotor position in order to obtain an average torque angle as close as possible to the ideal 90 electrical degrees. If the rotor is initially aligned with one of the excitation steps, then the torque angle is 120º at the beginning of the first step and it reaches 60º at the end of the excitation period.

4.3.3. Calculation of Incomplete First Step During Start-Up

The first step duration should be modified according to the initial rotor position when the rotor is not perfectly aligned with a step. For example, if the initial inductive sense result θ_{S0} is between 0º (step-0) and 60º (step-1), then step-2 is the first commutation step, and the step duration should be calculated to obtain $60º - \theta_{S0}$

rotation at the end of the excitation. The offset position $\Delta\theta_{S0}$ is calculated depending on the initial rotor position θ_{S0} that varies between $0°$ and $360°$ in an electrical cycle.

$$\Delta\theta_{S0} = \theta_{S0} - 60° \; floor(\theta_{S0}/60°) \tag{4.8}$$

where, $floor(\theta_{S0}/60°)$ gives the closest integer less than $\theta_{S0}/60°$. The first step time T_{X1} that results in $60°-\Delta\theta_{S0}$ rotation angle is

$$T_{X1} = \sqrt{\frac{60° - \Delta\theta_{S0}}{60°}} \; T_{LUT}[1] \tag{4.9}$$

where, $T_{LUT}[1]$ is the first step duration in the look-up table calculated for a complete $60°$ rotation.

The step durations following the first step should also be modified according to the angular velocity $\omega_2 = \alpha T_{X1}$ obtained after the first step. For $k>1$, the total angular motion θ_{sum} after the first step and before the k'th step is related to the elapsed time T_{sum} during the same period:

$$\theta_{sum} = (k\text{-}2)60° = \omega_2 T_{sum} + \frac{\alpha}{2} T_{sum}^2 \tag{4.10}$$

Solution of this second order polynomial is given by

$$T_{sum} = \frac{\sqrt{\omega_2^2 + 2\alpha(k\text{-}2)60°} - \omega_2}{\alpha} \; . \tag{4.11}$$

Angular velocity right before the k'th step is

$$\omega_k = \omega_2 + \alpha T_{sum} = \sqrt{\omega_2^2 + 2\alpha(k\text{-}2)60°} \tag{4.12}$$

Then, the duration T_{Xk} of the k'th step is obtained by solving:

$$60° = \omega_k T_{Xk} + \frac{\alpha}{2} T_{Xk}^2$$
$$= \sqrt{\omega_2^2 + 2\alpha(k\text{-}2)60°} \; T_{Xk} + \frac{\alpha}{2} T_{Xk}^2 \tag{4.13}$$

$$T_{Xk} = \frac{\sqrt{\omega_2^2 + 2\alpha(k\text{-}1)60°} - \sqrt{\omega_2^2 + 2\alpha(k\text{-}2)60°}}{\alpha} \tag{4.14}$$

The calculation of square root of a number by using floating point arithmetic operations may require too much processing time in a simple microprocessor as the step durations decrease depending on the rotor acceleration. It is possible to interpolate the step durations without significant error in the acceleration profile after the second step. The second step duration T_{X2} should still be calculated separately by solving:

$$60° = \omega_2 T_{X2} + \frac{\alpha}{2} T_{X2}^2 \tag{4.15}$$

$$T_{X2} = \frac{\sqrt{\omega_2^2 + 2\alpha 60°} - \omega_2}{\alpha} . \tag{4.16}$$

Other step durations for $k > 2$ can be found by interpolating the values available in the look-up table $T_{LUT}[.]$:

$$T_{Xk} = \frac{\theta_{S0} T_{LUT}[k\text{-}1] + (60° - \theta_{S0}) T_{LUT}[k]}{60°} . \tag{4.17}$$

The step durations obtained through interpolation result in less than 1.5º error in the rotation angle compared to the ideal 60º rotation expected in each commutation step.

4.3.4. Start-up Under Varying Load Conditions

With an unknown but constant load torque, it is necessary to drive and accelerate the motor until sufficient BEMF signal is obtained for synchronous operation.

Blind commutation step durations cannot be calculated accurately when the load torque is unknown. If the steps are too short, then the motor cannot keep up with the

commutation timing. If the steps are too long, then the motor may start back rotation. In any case, the motor may stop completely, or at least it may stall a few times during acceleration.

The driver can detect rotor position with inductive sense method after applying one or two commutation steps. An estimate of the load torque is obtained according to the measured rotor acceleration, and the duration of future commutation steps are calculated according to this estimate. The inductive sense position detection can be repeated to assure proper rotor acceleration.

The first blind commutation step is applied assuming that there is no additional load on the rotor. The expected angular acceleration is α_{ex}, and the expected change in angular position is

$$\Delta\theta_{ex} \ = \ \frac{\alpha_{ex}}{2} \, T_{X1}^2 \qquad\qquad (4.18)$$

where, T_{X1} is the first step duration calculated for the target acceleration α_{ex}. The actual change in angular position $\Delta\theta_{act}$ is found by using inductive sense method after the first step. The actual acceleration α_{act} with additional load is given by

$$\alpha_{act} \ = \ \frac{2 \, \Delta\theta_{act}}{T_{X1}^2} \, . \qquad\qquad (4.19)$$

A modified step duration T_{X1act} is required in order to obtain complete $\Delta\theta_{ex}$ rotation when the target acceleration is α_{act}. T_{X1act} can be found as follows.

$$\Delta\theta_{ex} \ = \ \frac{\alpha_{act}}{2} \, T_{X1act}^2 \ = \ \frac{\Delta\theta_{act}}{T_{X1}^2} \, T_{X1act}^2 \qquad\qquad (4.20)$$

$$T_{X1act} \ = \ T_{X1} \sqrt{\frac{\Delta\theta_{ex}}{\Delta\theta_{act}}} \qquad\qquad (4.21)$$

The blind commutation algorithm completes the first excitation step by applying an additional step duration given by $T_{X1act} - T_{X1}$ before it proceeds to the second step.

After applying the first step, the scaling factor is calculated according to the actual angular rotation since the beginning of blind commutation.

$$F_{TXS} = \sqrt{\frac{\Delta\theta_{ex}}{\Delta\theta_{act}}} \qquad (4.22)$$

If the rotation angle expected in the k'th step is 60°, then the k'th step duration T_{Xk} is given by

$$T_{Xk} = F_{TXS} \, T_{LUT}[k] \qquad (4.23)$$

If the required k'th rotation angle $\Delta\theta_k$ is different than 60°, then the k'th step duration T_{Xk} should be calculated depending on the total excitation time T_{Sact} and the total rotation angle θ_{act} determined by inductive sense before the k'th step.

$$T_{Sact} = \sum_{i=1}^{k-1} T_{Xi}, \qquad \alpha_{act} = \frac{2\,\theta_{act}}{T_{Sact}^2}, \qquad \omega_k = \alpha_{act}\,T_{Sact}. \qquad (4.24)$$

where T_{Sact} is the total excitation duration since the beginning of blind commutation. T_{Xk} is found by solving

$$\Delta\theta_k = \omega_k T_{Xk} + \frac{\alpha_{act}}{2}\,T_{Xk}^2 \qquad (4.25)$$

$$T_{Xk} = \frac{\sqrt{\omega_k^2 + 2\alpha_{act}\Delta\theta_k} - \omega_k}{\alpha_{act}} = \sqrt{T_{Sact}^2 + 2\Delta\theta_k/\alpha_{act}} - T_{Sact} \qquad (4.26)$$

The start-up algorithm for varying load conditions is summarized below.

1. Apply the first step with the duration $T_{LUT}[1]$.
2. Detect actual rotation angle θ_{act} obtained since the beginning of blind commutation with inductive sense.
3. Calculate actual acceleration α_{act} based on θ_{act}.
4. Check the angular position error $\theta_{err} = \theta_{act} - (k-1)60°$:
   4.1. If rotor moved more than expected ($\theta_{err} > 0°$), then reduce the rotation angle expected in the k'th step:
   $\Delta\theta_{Xk} = 60° - \theta_{err}$

4.2. If rotor moved less than expected, then check if it is necessary to complete the $k-1$'st step before proceeding to the k'th step. If $\theta_{err} < -10°$ then complete the $k-1$'st step:
$$\Delta\theta_{Xk\text{-}1} = -\theta_{err}$$
4.3. If $-10° < \theta_{err} < 0°$ then extend the rotation angle expected in k'th step:
$$\Delta\theta_{Xk} = 60° - \theta_{err}$$
5. Calculate the scaling factor F_{TXS} for the excitation step durations according to θ_{act}.
6. Calculate the duration T_{Xk} or $T_{Xk\text{-}1}$ of the next excitation
7. Repeat the algorithm for 5 steps until the first 3 or 4 excitation steps are completed. Afterwards, use the lookup table $T_{LUT}[k]$ scaled by the factor F_{TXS}. Step durations should be extended by another 2%-5% to have the necessary safety margin during acceleration. For example, $T_{Xk} = 1.05\ F_{TXS}\ T_{LUT}[k]$ after the first 3 or 4 excitation steps period.

The actual acceleration α_{act} can be the result of either some additional constant loading torque τ_{add} or some additional rotational inertia M_{add} on the rotor. In the first case, the actual torque τ_{act} acting on the initial rotational inertia M_0 and the resultant acceleration α_{act} are given by

$$\tau_{act} = \tau_m - \tau_{load} \tag{4.27}$$

$$\alpha_{act} = \frac{\tau_{act}}{M_0} \tag{4.28}$$

where, τ_m is the torque generated by the motor which is assumed to be a constant. In the second case, the actual acceleration is

$$\alpha_{act} = \frac{\tau_m}{M_0 + M_{add}} \tag{4.29}$$

which is also a constant. An additional constant torque is required to accelerate the additional inertia. In other words, the presence of additional loading torque or additional inertia makes no difference as long as the purpose of blind commutation is to obtain a constant acceleration profile.

4.4. Implementation of Driver Synchronization

The purpose of synchronization is to determine commutation timing according to the rotor position and speed after the blind commutation. If the blind commutation is successful, then the rotor can keep up with the driver, but the rotor position related to driver steps can be off by +/-1 step.

The driver cannot determine timing of commutation steps and BEMF ZC detection windows after the blind commutation stage. Driver synchronization is achieved by detecting two ZCs that allow estimation of rotor speed and position. Motor driver outputs are 3-stated after blind commutation to be able to detect two ZCs. If these two ZCs are not detected, or time between the two ZCs is far from the expected ZC period, then these indicate a startup failure.

Experiments have been carried out on the test setup to verify the synchronization function. The results of these experiments are shown in Figure 4.5, Figure 4.6 and Figure 4.7. Figure 4.5, shows whether the motor reaches the step time value given in blind commutation or not. Figure 4.6 and Figure 4.7, show that ZC points can be read three times or once in an electrical cycle. If ZC point is to be read once, then the next ZC point of the falling edge on the same phase will be seen after 6 steps. In this case the motor should wait for 1 electrical cycle (360 electrical degrees). On the other hand, if ZC point is read from three phases, then the motor detects falling edges after every 120 electrical degrees. Therefore, synchronization is completed in a shorter time.

The motor speed obtained from ZC timing was compared with the motor speed expected as a result of the duration of the last blind commutation step. As seen from Figure 4.5, the expected speed at the end of blind commutation is 5ms. During synchronization part, the cycle time was obtained at 33.2 ms and the resultant average step time is 5.53 ms. As seen below, CH1 probe is a marker that indicates the time between two ZCs and CH2 probe is the output of external BEMF detector.

Figure 4.6 shows single ZC detection in an electrical cycle, where the second falling edge is detected on phase C again. In Figure 4.7, three ZCs are detected, and phase-A is monitored for the next falling edge. The CH2 probe is voltage of phase C, and CH1 probe is a marker signal used as a trigger at the end of blind commutation.
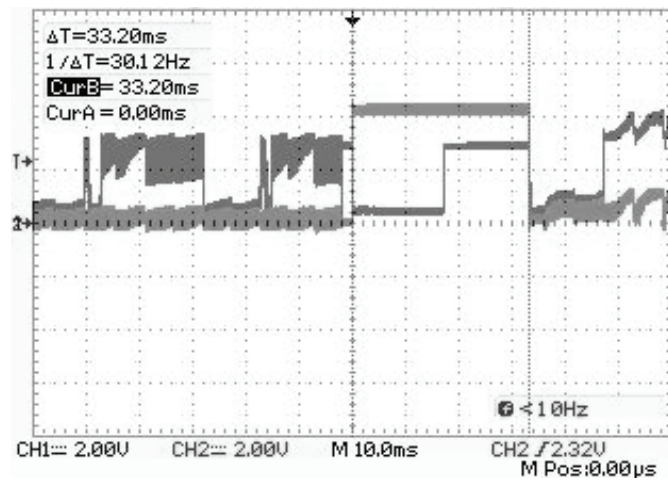
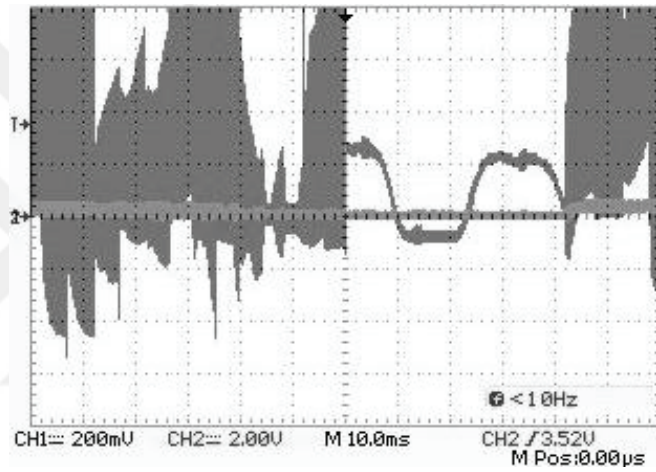Figure 4.5. Compare motor speed with the last delay of blind commutation.

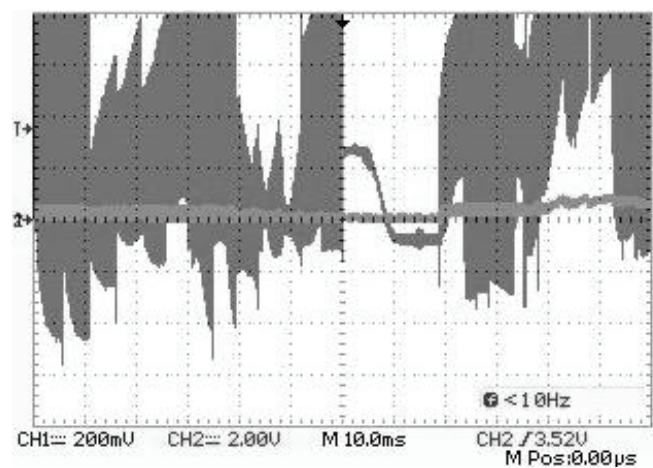Figure 4.6. 1-ZC detection at synchronization part.

Figure 4.7. 3-ZC detection at synchronization part.

4.5. Implementation of Synchronous Commutation

The initial commutation steps for synchronous commutation are calculated based on the ZC times obtained in the synchronization stage. Afterwards, commutation timing is updated after every ZC detection during synchronous commutation. A ZC detection window is opened right before the expected ZC time based on previous timing data. In the detection window, BEMF signal is received from 3-stated winding, while PWM switching on the other two windings is suspended. PWM switching is stopped in detection window, to prevent false ZC detections caused by switching noise. The period without PWM that starts right before the expected ZC transition is called ZC detection window. There are three options to hold the PWM waveform in the ZC detection window:

1. One winding is 3-stated while the other two are pulled to ground
2. One winding is 3-stated while the other two are pulled to supply and ground
3. All windings are 3-stated.

One of these options is implemented by using ADC sampling or the external comparator. In addition, motor speed is regulated by a controller during synchronous commutation. Typically, a PI (Proportional-Integral) controller calculates the PWM duty cycle.

4.5.1. BEMF Detection at High Speed with ADC Channel

Detection of ZC is expected in the middle of a commutation step for constant speed or small changes in speed. In order to find proper commutation step during BEMF sense, two timers are used to measure the time from beginning of a commutation step to ZC detection and from ZC detection to the next step. In this setup, Timer-4 and Timer-1 are used for measuring time as shown in Figure 4.8. Timer 4 has the ability to generate 3 PWM outputs and its overflow interrupt is used to check BEMF sense signal via ADC unit. On the other hand, Timer-1 is used to measure timing between points of first commutation to ZC detection and from ZC to the next commutation respectively (Atmel AVR498 2009).
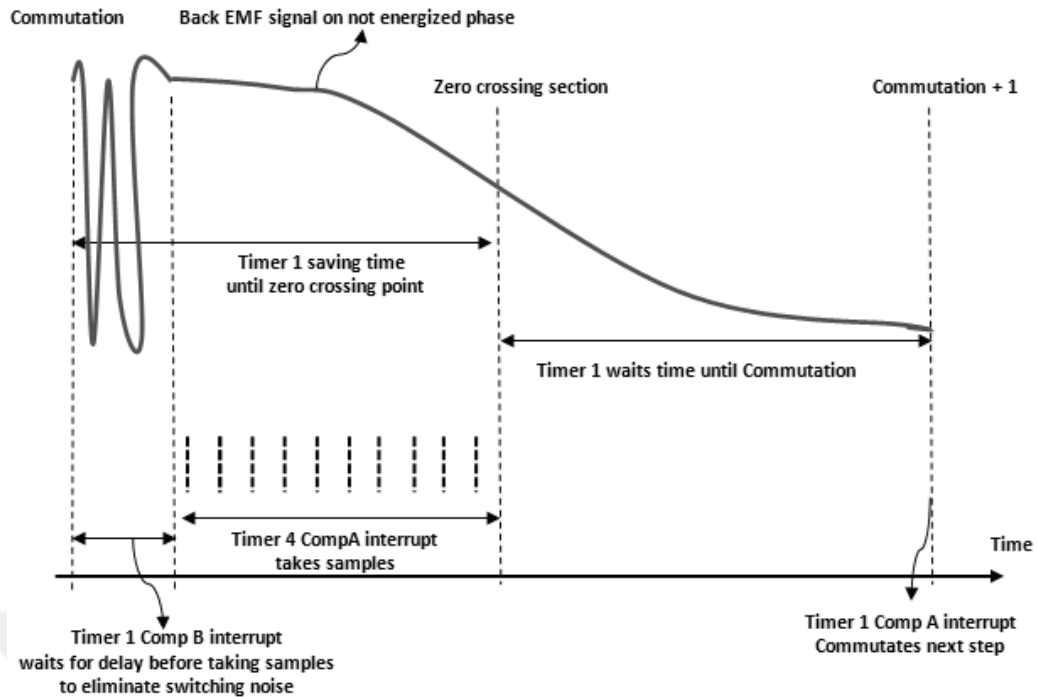
Figure 4.8. Timer usage for ZC detection.

Timer-1 prescaler is selected as 64 to measure time up to 262.14 ms with 4 μs resolution. The timer-1 compare-A interrupt commutates the step at scheduled time. Compare-B interrupt is used to obtain a time delay before taking samples in order to avoid switching noise. Timer-4 prescaler is selected as 1 to measure time durations up to 4.095 ms with 0.0625 μs resolution. Compare-A interrupt of timer-4 triggers acquisition of samples from floating phase with ADC. Timer 5 is used for PWM waveform generation to drive MOSFETs with 8-bit phase-correct PWM mode. The algorithm for BEMF zero-cross detection with ADC channel is summarized below.

- **Compare-A interrupt of Timer-4 waits**
  - Registers are defined
  - Clear all interrupt flags of timer-4
  - Close PWM operation, use PORTL operation only
  - 10 us delay before taking sample
  - Read BEMF signal via ADC
  - Check if estimation polarity and BEMF value are suitable
  - If YES (either rising or falling edge of BEMF signal)
    - Save timing of BEMF detection via timer-1 register (TCNT1)
    - Clear timer-1 register
    - Define commutation time
    - Set timer-1 comparison A interrupt
    - Clear timer-1 interrupt flags
    - Disable all timer-4 interrupt
    - Clear ZC errors
    - Wait for the interrupt

49

- o If NO
  - ▪ Counting ZC error then try again to find zero cross section
  - ▪ If zero cross errors are too much "400 for instance".
  - ▪ Close all the interrupts and start from the beginning.
  - ▪ Wait for interrupt in the main function
- **Compare-A interrupt of Timer-1 waits**
  - o Clear all the interrupt flags of timer-1
  - o Commutate next commutation step with PWM operation
  - o Clear timer-1 to start measurement for time since commutation
  - o Define polarity of BEMF (Rising or falling)
  - o Define ADC channel
  - o Preparation for next step, increment next commutation variable
  - o Disable all timer-1 interrupts
  - o Open timer-1 compare B interrupt for delay to avoid switching noise
  - o Wait for interrupt in the main function
- **Compare-B interrupt of Timer-1 waits**
  - o Clear all interrupt flags of timer-1
  - o Disable timer-1 interrupt
  - o Set timer-4 compare A interrupt to take sample
  - o Clear timer- 4
  - o Wait for interrupt in the main function

A test was implemented on BLDCM-1 by using BEMF detection algorithm with the ADC sampling. In Figure 4.9, the commutation points are shown on the BEMF signal. The ZC detection in the falling edge and rising edge of the BEMF signal is shown in Figure 4.10, Figure 4.11 and Figure 4.12. CH1 probe shows the ADC process and CH2 probe shows BEMF signal.
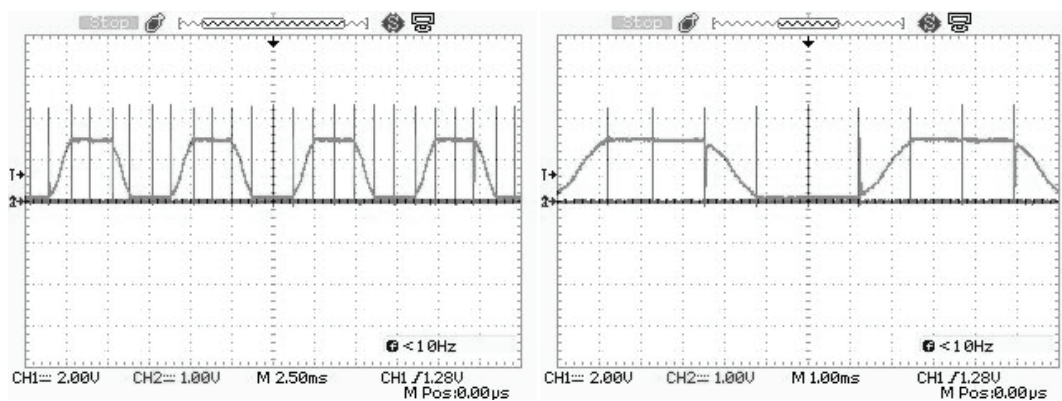

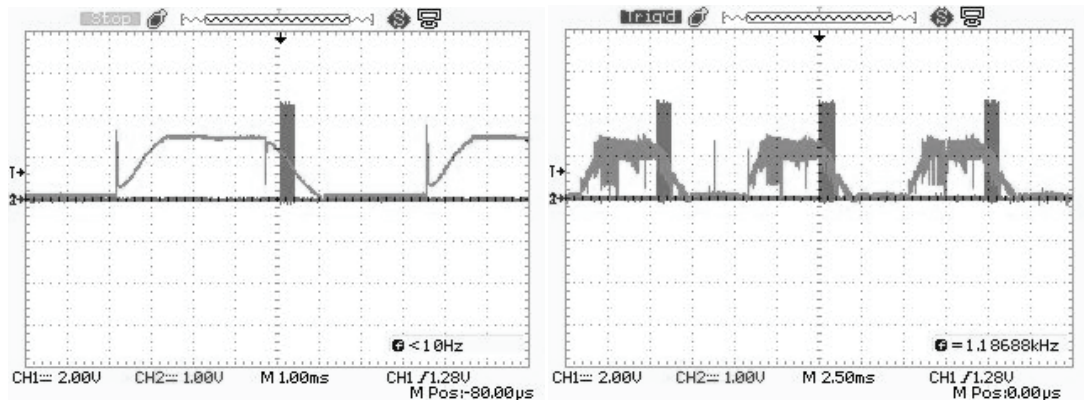Figure 4.9. Commutation Marker at %100 duty cycle.

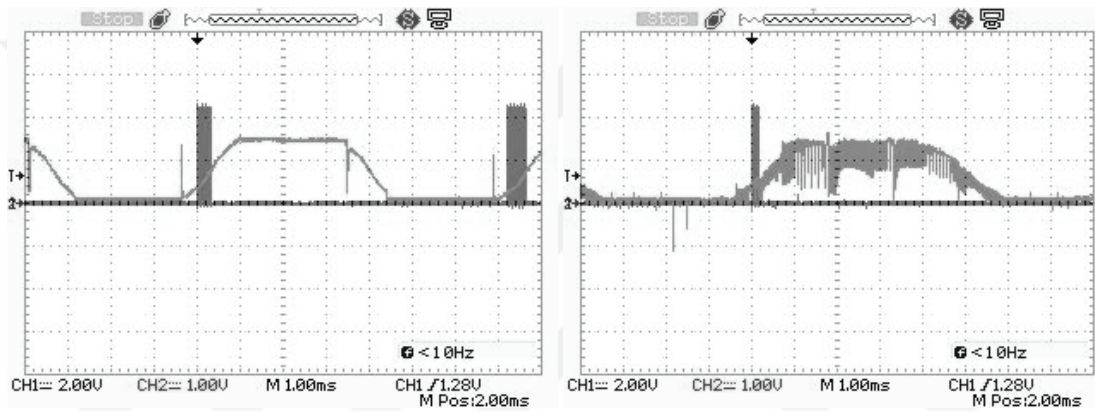Figure 4.10. ZC marker on falling edge at %100 PWM and %40 PWM.

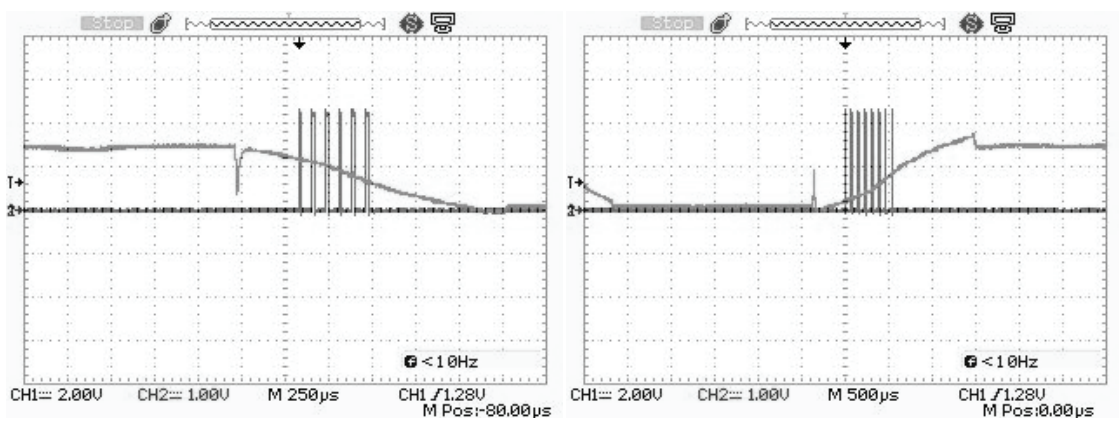Figure 4.11. ZC marker on rising edge at %100 PWM and %40 PWM.

Figure 4.12. Falling edge and rising edge threshold is arranged separately.
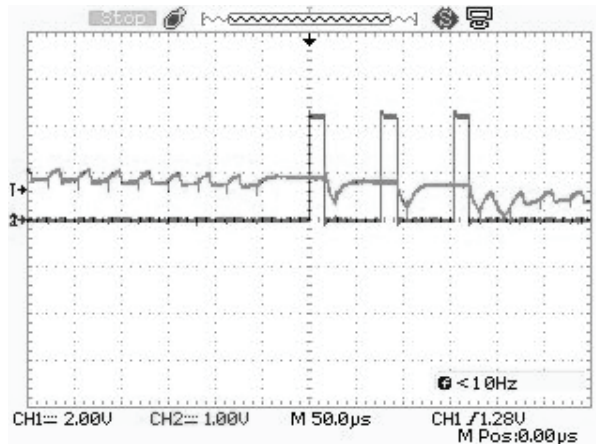
Figure 4.13. Time delay to avoid switching noise.

In conclusion, BEMF detection with ADC channel can be used to perform BLDC driving. BEMF signal is scanned by ADC in order to find ZC point at rising edge or falling edge. The driving of the motor is tested with the help of a specific algorithm. No external components were used, because BEMF signal processing was completed with the aid of the ADC channels on ATmega2560, which is used as a controller. One of the difficulties encountered was, the distortion on the BEMF signal during MOSFET switching. In order to deal with BEMF signal distortion, ADC sampling is delayed as seen in Figure 4.13. The CH2 probe is voltage of phase C, CH1 probe is a marker showing ADC reading process.

4.5.2. BEMF Detection at High Speed with External Comparators

With the help of the external comparator, the status of BEMF signal can be checked in a shorter time to find ZC points. For this, the circuit described in BEMF detection section of chapter 3 is used.

To read the BEMF signal, a window is opened during the commutation and the BEMF signal is read through this window to check if it arrives at the expected time. The shorter this window pops up, the more controllable is the power transferred to the motor. When the window is open, the motor does not take voltage in the range because the phases are not taking desired voltage.

In conclusion, BEMF detection is completed with the external comparators. BEMF signal is waited during ZC window time which is selected according to step

time. For instance, ZC sensing window is tested with 2^2, 2^3, 2^4, and 2^5 window scale divider or window being fully opened. These changes are also applied on a different sensing mode. Sensing mode organizes the output waveform of the controller. When zero crossing window is open, the sensing process starts. Experimental results are shown in Chapter 5.

4.6. Monitoring System

This section has been prepared to summarize the use of experiments and to understand how to work with codes. Briefly, microcontroller is accessed and processed through this interface. The LabVIEW screenshot shown in Figure 4.14, displays the events that are happening during experiment (i.e. results and commands which are controlled via serial communication).

There are several parts on the monitoring system to rotate BLDCM appropriately. The following explanations introduce the monitoring system. The communication part includes command writing and monitoring data. `Init` button initializes the program. During initializing process, values on the screen are sent to the microcontroller automatically. Then, values that are to be changed are sent to the microcontroller after pushing the related button. LabVIEW is used for only data transfer and monitoring. The commutations and control processes are performed by the microcontroller.

The part of inductive sense, shows the rise time for six steps. The minimum step and electrical angle values are visible after pushing the inductive sense button. The reference voltage of external comparator for threshold can be set in this part in 0 to 255 range. This setting controls the PWM output. After low pass filter, the analog signal is used as the threshold for the external comparator.

The excitation step during desired time with desired PWM value can be arranged in the alignment part that includes step selection, time duration, and duty cycle value. This part is used for testing inductive sense and excitation step accuracy.
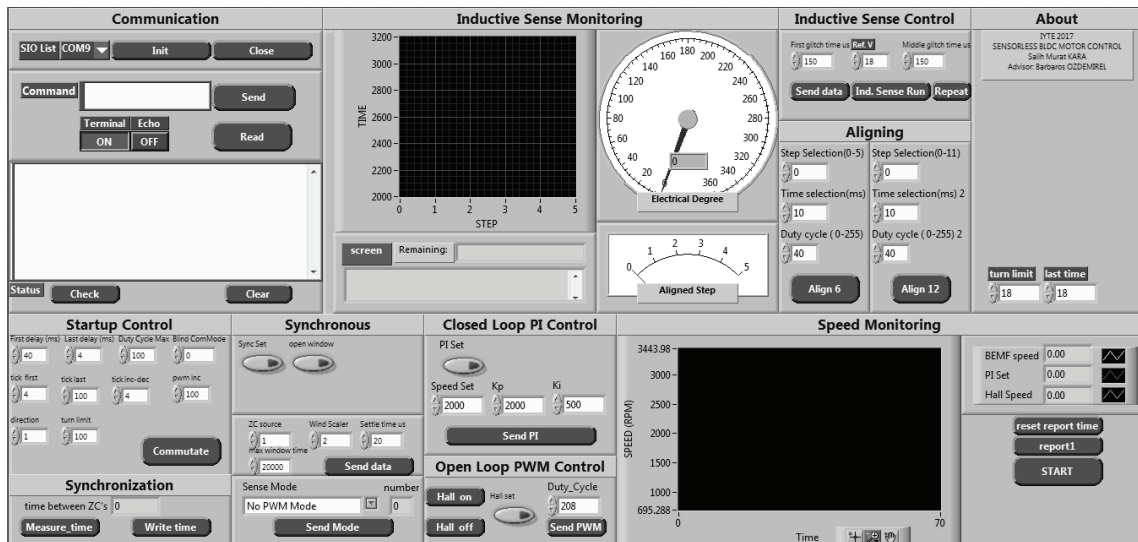
Figure 4.14. LabVIEW user interface.

After testing inductive sense and excitation step accuracy, motor start-up mode based on the output load can be selected at the start-up control part. In this part, first and last step durations, and PWM duty cycle for blind commutation can be set. Blind commutation starts with inductive sense algorithm, then calculates the next steps. At the end of the blind commutation the function returns BCdone which is equal to 1.

Synchronization part determines the time between two ZCs. Two ZC falling edges are detected with the external interrupt (INT0). The external interrupt service routine counts the coming interrupt. When the first interrupt is received, the timer starts counting, and it stops when the second interrupt arrives. The measured time between the two ZCs gives the duration of one electrical cycle. At the end of this process synchronization function sends the SYNCdone which is equal to 1.

If Sync Set button is active, synchronous commutation starts after synchronization part is done. Variable BEMF sensing window can be activated with a control button, or if the button is disabled, window duration is fixed at maximum. The last option selects the drive mode during BEMF sense to see their performances. The available drive modes are Coasting run, No PWM, and Brake mode. While the BEMF window is open, coasting run mode disconnects all MOSFETs. Therefore, controller three states all phases, and the BEMF signal in related phase can be observed. No PWM mode holds the voltage constant at maximum level. The brake mode pulls the driven phase to the ground excluding the sensing phase.

There are two options used to control motor speed and these are, closed loop, and open loop control systems. Open loop control runs the motor with PWM without checking the motor speed. If `PI Set` is enabled, PI algorithm works and the motor speed is regulated. Ki, Kp and speed set parameters can be arranged in this part.

Speed monitoring shows the speed setting and the actual motor speed in RPM while the start button is active. The functions implemented for speed control and monitoring are summarized below.

- `Blind_commutation:` This function starts with inductive sense and accelerates the motor. At the end of this function <u>BCdone</u> flag is set.
- `Synchronization:` If <u>BCdone</u> is set, then synchronization function enables the external interrupt to catch ZC points on falling edge of BEMF. When the first ZC arrives, the timer starts to count until the second ZC detection. After the second ZC detection, the process is done and the <u>SYNCdone</u> flag is set at the end of the function.
- `Synchronous_commutation:` If <u>SYNCdone</u> flag is set, then the synchronous function of the related ISR vector is enabled. This ISR executes the motor at scheduled time. At the detection step, ZC window opens and waits for the ZC point. If it is obtained, the <u>ZCfound</u> flag is set.
- `PIcontrol_calc:` If <u>ZCfound</u> is set, PI algorithm determines the PWM output according to internal speed information.

4.7. Difficulties Encountered

There are several challenges that were encountered during BLDCM controller implementation and they are summarized below.

4.7.1. Center Tap Connection

Normally, BEMF signal is detected between the center tap of motor windings and one of the 3-stated connections. If the motor center tap connection is not available, then there are two options. First, only one motor winding is 3-stated, and the other two windings are kept at a constant voltage during BEMF detection. This can be done for short periods of time while ZC detection windows are open during synchronized commutation. On the other hand, connecting two of the motor windings to constant voltage for an excessive time changes motor timing during synchronization. Grounding two windings will apply a brake to the rotor. If one of the windings is connected to a voltage supply, then the rotor may accelerate or decelerate as a result of the generated torque. Second, a virtual center tap can be obtained by connecting three resistors in Y

configuration between the motor terminals. BEMF signal can be detected between a center node of the three resistors and one of the motor windings when all three driver outputs are 3-stated.

4.7.2. ZC Inaccuracy

ZC timing changes from one electrical cycle to another in a mechanical revolution. Similarly, the times between the ZCs detected on three motor windings are different in an electrical cycle. These timing errors are caused by imperfect positioning of rotor and stator magnetic poles. The speed measurements using ZC timing of different phases and different electrical cycles give wrong results unless the timing of all ZC periods is calibrated.

It is not necessary to detect all six ZCs in an electrical cycle. In ordinary motor control applications, one ZC detection in an entire mechanical cycle is sufficient to determine the motor speed.

4.7.3. ZC Detection Window Affects Motor Torque

Keeping two of the motor windings at constant voltage means applying either 0% PWM (braking) or 100% PWM (full acceleration) for the duration of ZC detection window. These changes in the PWM waveform can affect the speed control. As a solution, duration of detection windows can be reduced at high speeds, because high BEMF strengths allow ZC detection in a shorter time.

4.7.4. Slope and Noise at Low Speed

BEMF signal is not sufficient at low speed. Hence motor needs some minimum speed to detect ZC points. Moreover, BEMF signal has noise due to switching. These noisy signals cause wrong ZC detection unless a proper measurement zone or a good filtering method is chosen.

CHAPTER 5

RESULTS AND DISCUSSION

Experimental results obtained in laboratory studies with two different types of BLDC motors are presented in this chapter. The angular position measurements by using inductive sense method are discussed in the first section followed by the speed regulation results based on BEMF detection at high speeds. In the last section, motor start-up experiments with six different load conditions are presented.

5.1. Position Detection Results with Inductive Sense

Two verification tests were done to measure the accuracy of the inductive sense position detection:

1. Checking motor accuracy: The rotor is aligned at the first step (A=>B) and the rotor position is marked as 0 degree of mechanical angle. Then the rotor is aligned with all 12 electrical steps and the mechanical angle in a revolution is recorded. Electrical step angles as a function of mechanical angle are plotted. Experiments were performed on two different BLDC motors (BLDCM-1 and BLDCM-2) and the results are shown in Figure 5.1 and Table 5.1. The alignment position of the implemented motor steps and the inductive sense results of these positions are presented.
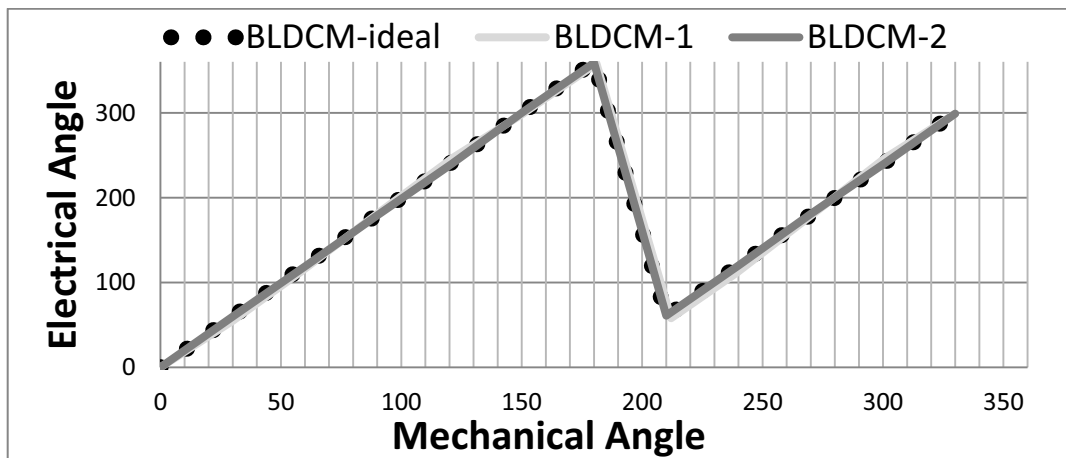

Figure 5.1. Electrical step angles as a function of mechanical angle.

Table 5.1. Electrical and mechanical angles against the applied electrical steps.

Electrical Steps	BLDCM-ideal		BLDCM-1		BLDCM-2	
	Electrical Angle	Mechanical Angle	Electrical Angle	Mechanical Angle	Electrical Angle	Mechanical Angle
0	0	0	0	0	0	0
1	60	30	55	30	62	31
2	120	60	112	58	121	61
3	180	90	183	91	179	90
4	240	120	248	122	240	121
5	300	150	298	150	300	150
0	360-0	180	358	181	359	180
1	60	210	58	212	61	210
2	120	240	111	239	120	240
3	180	270	181	271	181	270
4	240	300	247	301	241	301
5	300	330	297	329	299	330

2. Checking inductive sense accuracy: The rotor is manually aligned at 10 degree steps starting at 0 degree mechanical angle, and the inductive sense results are recorded. Experiments were performed on two different BLDC motors (BLDCM-1 and BLDCM-2) and the results are shown in Figure 5.2, and Table 5.2 where the inductive sense results are given as a function of mechanical angle.
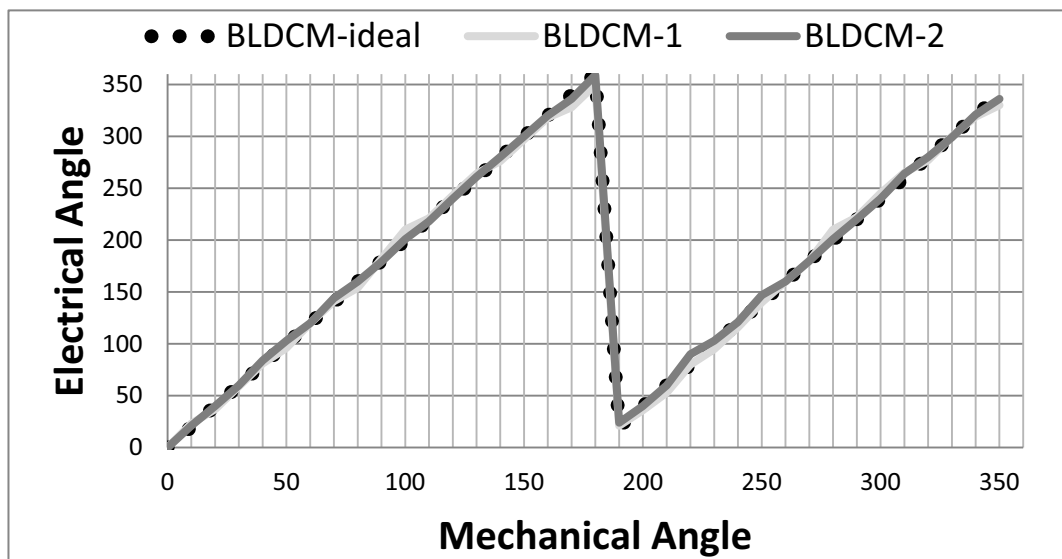

Figure 5.2. Inductive sense results as a function of mechanical angle.

Table 5.2. Inductive sense results as a function of mechanical angle.

| Mechanical Angle	BLDCM-ideal		BLDCM-1		BLDCM-2	
	Electrical Angle	Mideal - Error	Electrical Angle	M1-Error	Electrical Angle	M2-Error
0	0	0	0	0	0	0
10	20	0	23	-3	21	-1
20	40	0	37	3	40	0
30	60	0	59	1	60	0
40	80	0	81	-1	84	-4
50	100	0	96	4	103	-3
60	120	0	120	0	120	0
70	140	0	141	-1	144	-4
80	160	0	154	6	160	0
90	180	0	182	-2	179	1
100	200	0	210	-10	201	-1
110	220	0	221	-1	218	2
120	240	0	243	-3	240	0
130	260	0	264	-4	261	-1
140	280	0	276	4	280	0
150	300	0	297	3	300	0
160	320	0	318	2	320	0
170	340	0	328	12	336	4
180	360-0	0	350	10	359	1
190	20	0	21	-1	24	-4
200	40	0	36	4	40	0
210	60	0	53	7	60	0
220	80	0	80	0	90	-10
230	100	0	95	5	103	-3
240	120	0	116	4	121	-1
250	140	0	140	0	147	-7
260	160	0	160	0	160	0
270	180	0	180	0	180	0
280	200	0	210	-10	201	-1
290	220	0	222	-2	220	0
300	240	0	245	-5	240	0
310	260	0	265	-5	264	-4
320	280	0	277	3	280	0
330	300	0	300	0	299	1
340	320	0	319	1	321	-1
350	340	0	330	10	336	4
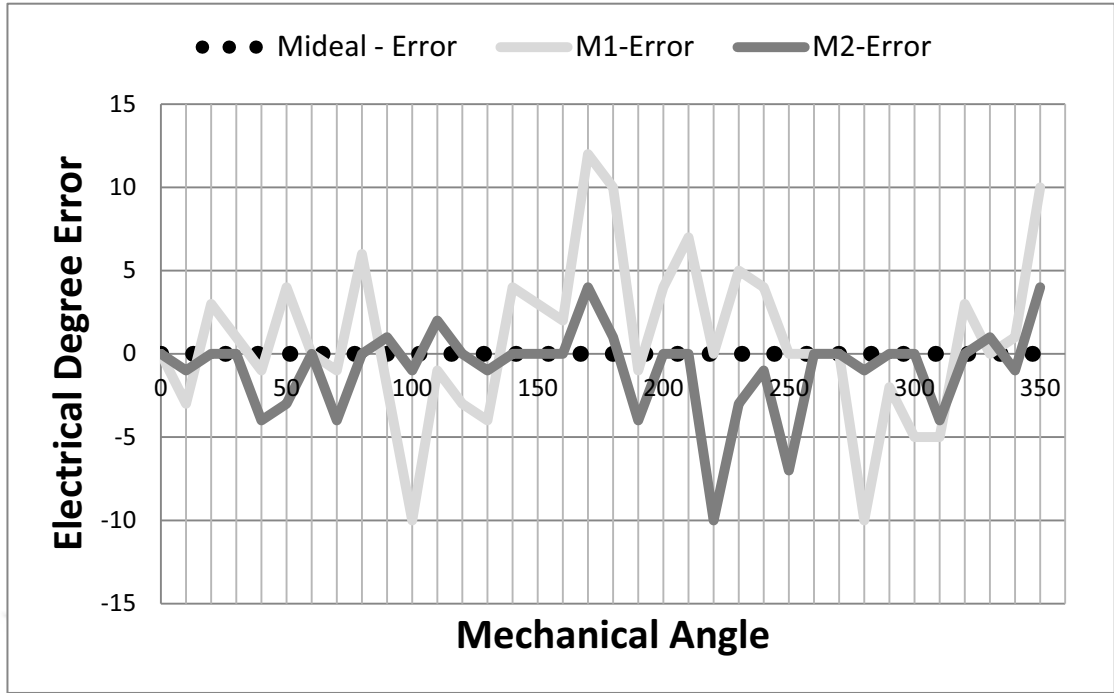
Figure 5.3. Position detection errors for BLDCM-1 and BLDCM-2.

The rotor position was found with maximum 12 degree error for BLDCM-1 and maximum 10 degree error for BLDCM-2. The resultant error graphs are shown in Figure 5.3.

5.2. Speed Regulation with BEMF Detection

Two features of speed regulation with BEMF detection was tested by monitoring the variable BEMF detection window and the PI controller response to step changes in target speed.

5.2.1. Variable BEMF Detection Window Test Results

A long BEMF detection window is required after the synchronization since there may be large variations in the ZC timing due to the low BEMF amplitude at low speeds. On the other hand, disabling driver outputs for excessive periods of time degrades the driver performance and causes additional mechanical vibrations. As a solution, the BEMF window duration is adjusted dynamically depending on the motor speed. The

BEMF detection algorithm determines the window duration with a scaling factor as a fraction of the commutation step duration, and the scaling factor is further reduced as the motor reaches its operational speed.

In order to adapt to the sudden speed changes due to varying load conditions, the BEMF detection algorithm automatically extends the window duration when it is not possible to detect a ZC within the allowed detection period. If changes in the motor speed are too much, then a ZC occurs either before or after the BEMF detection window. In that case, the detection algorithm doubles the scaling factor for the window duration until the ZC becomes visible again.

Window scale, settling time and sense mode are changed while monitoring ZC detection during synchronous mode. In order to analyze the effects of the changing ZC window scale and BEMF sense mode on ZC detection, various tests were performed in different sense modes and the results are shown in the following figures. CH1 probe shows ZC window and CH2 probe shows BEMF signal on phase-C, which is 3-stated while the window is open. As a result of the tests, it was observed that the ZC window range must be selected appropriately.
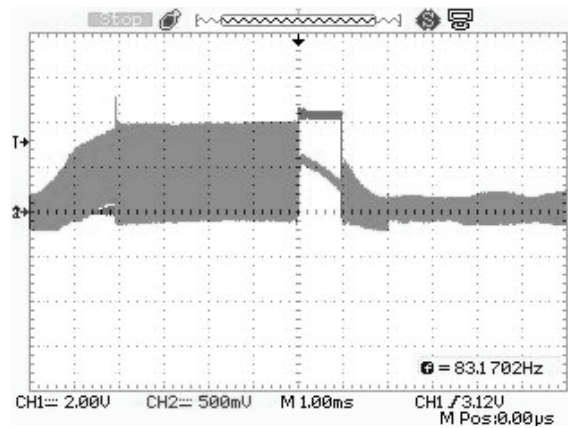

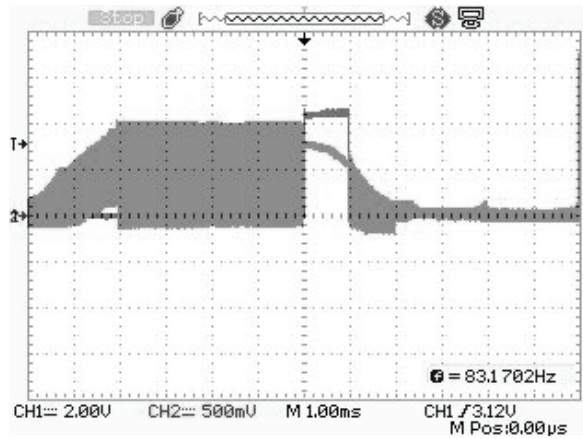Figure 5.4. Window fully opened with coasting sense mode.

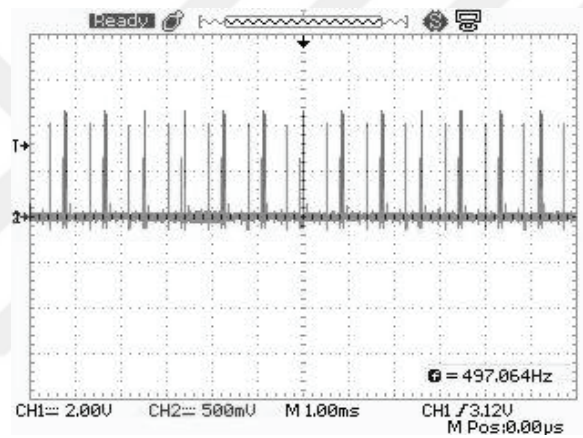Figure 5.5. Window fully opened with No PWM sense mode.

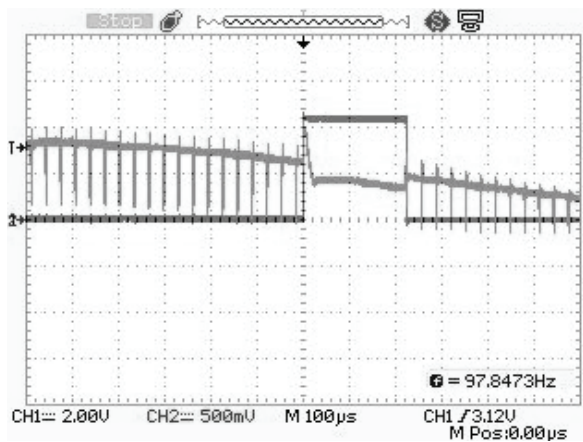Figure 5.6. Window fully opened with Brake sense mode.

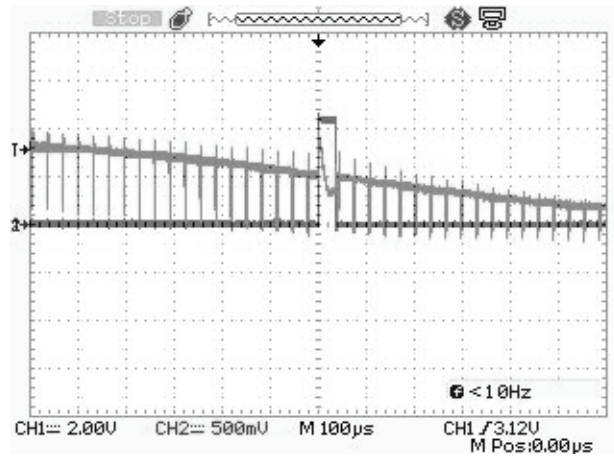Figure 5.7. Window scale divider is 2 in coasting sense mode.

Figure 5.8. Window scale divider is 3 in coasting sense mode.
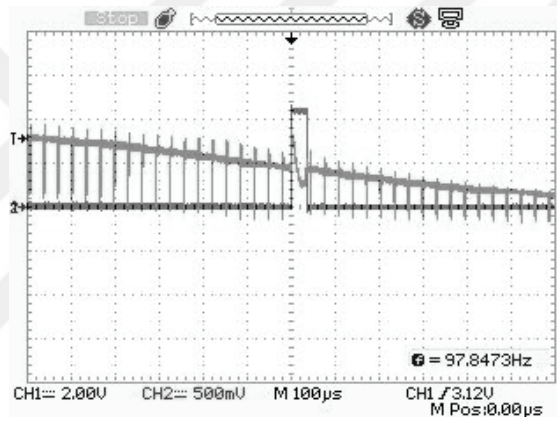

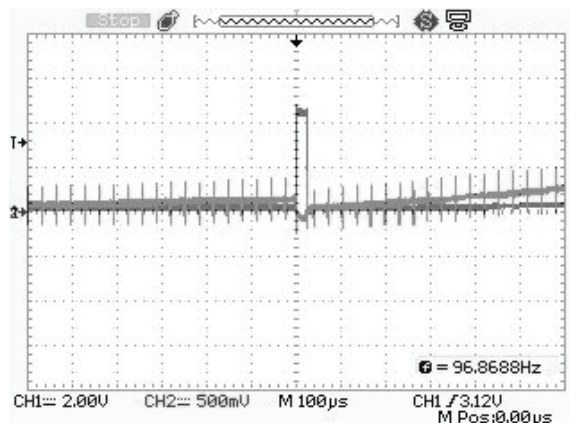Figure 5.9. Window scale divider is 4 in coasting sense mode.

Figure 5.10. Window scale divider is 5 in coasting sense mode.
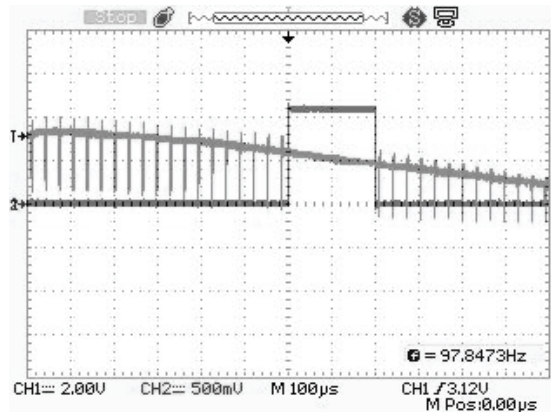
Figure 5.11. Window scale divider is 2 in no PWM sense mode.
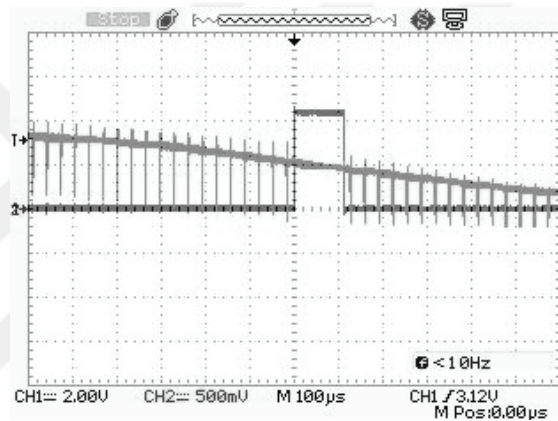

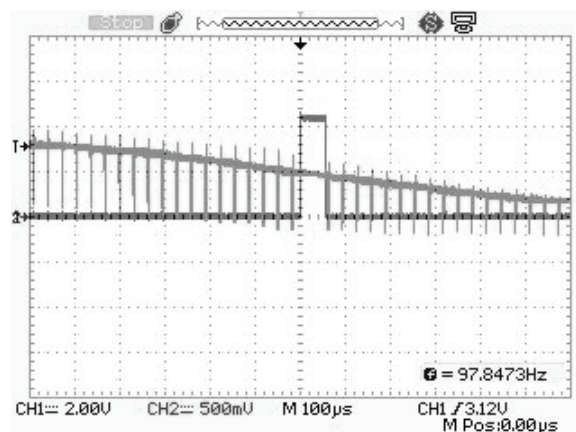Figure 5.12. Window scale divider is 3 in no PWM sense mode.

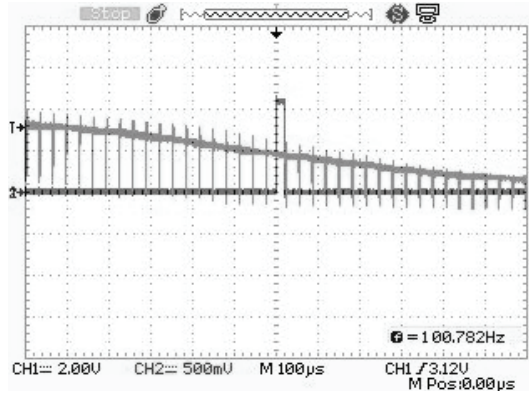Figure 5.13. Window scale divider is 4 in no PWM sense mode.

Figure 5.14. Window scale divider is 5 in no PWM sense mode.
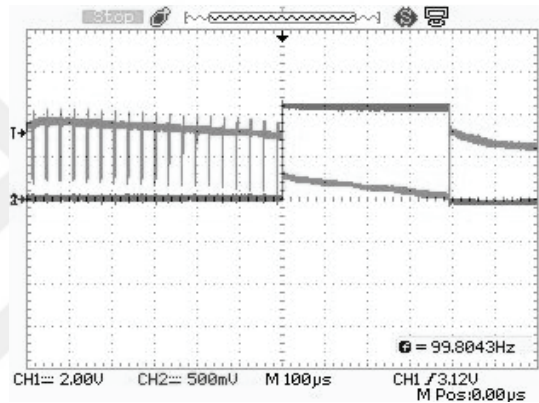
Figure 5.15. Window scale divider is 2 in brake sense mode.

5.2.2. PI Controller Step Response

In this section, test results of the developed software and hardware are given for speed regulation based on BEMF detection at high speeds on an unloaded motor. These experimental results are obtained with the BEMF detection circuit which was designed with external comparator. The motor is accelerated by using blind startup algorithm and the PI controller is activated after the synchronization.

Initially the target speed was set to 2700 rpm and the PI controller was given sufficient time until it stabilizes at this target. Afterwards, step changes were applied to the PI controller input to obtain 2400, 2000, and 3050 rpm target speed settings while the actual rotor speed was monitored on the LabVIEW window. The motor speed was

calculated once every revolution according to the BEMF ZC detection timing. The graph given in Figure 5.16 shows the target speed setting (PI SET) and the instantaneous speed measurements according to the BEMF signal and one of the hall-effect sensor outputs. The hall-effect sensor output was monitored just to verify the speed measurements based on BEMF detection, and the two resultant speed plots match each other as expected.
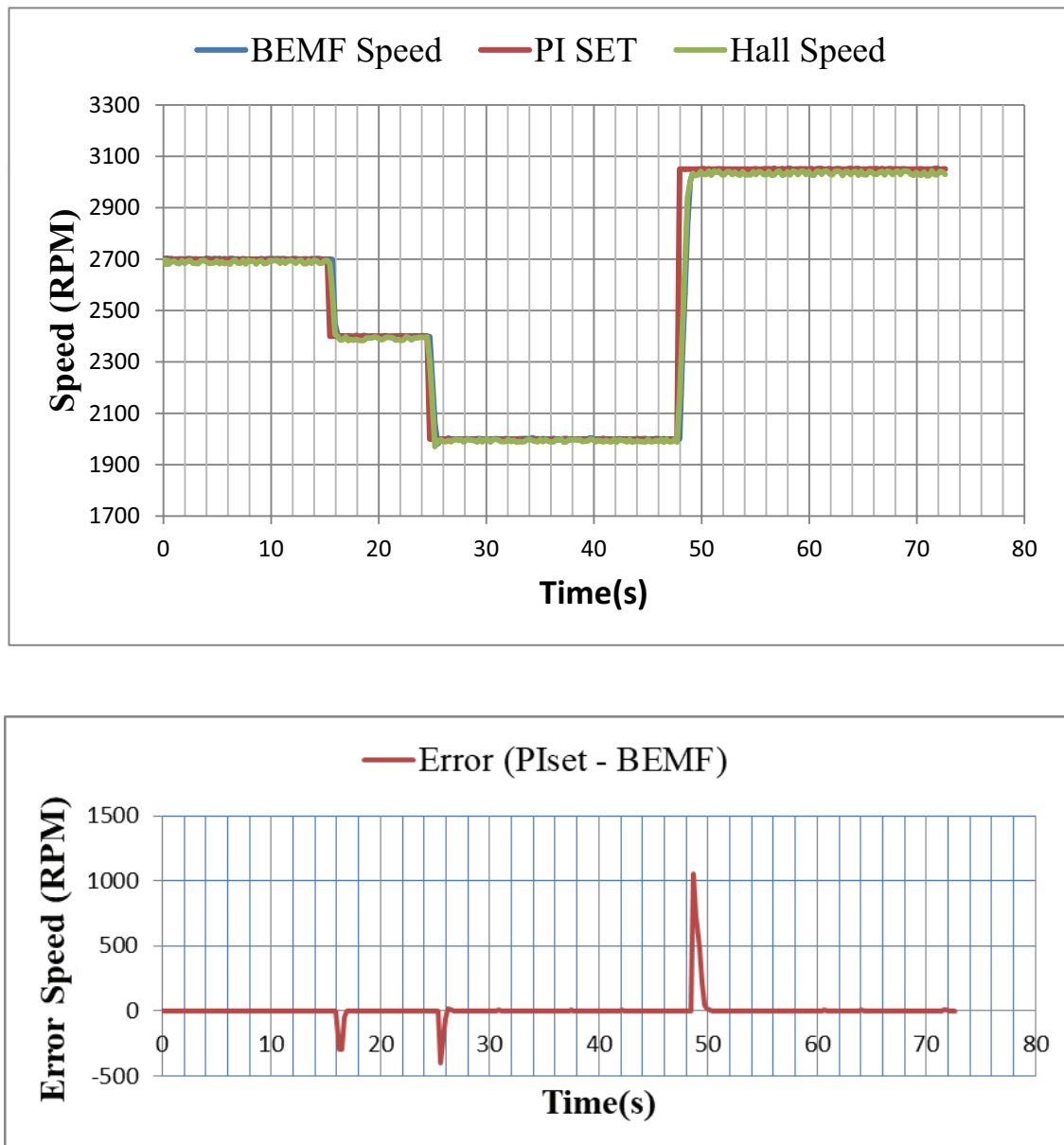

Figure 5.16. Speed Comparison.

As seen from the results, the driver maintained the proper commutation sequence and the actual motor speed followed the target speed setting. Proportional and integral gain coefficients of the PI controller were tuned to obtain a damped step response without causing an overflow at the controller output that determines the driver PWM duty cycle. The tuned coefficients were Kp = 2000 for the proportional and Ki = 500 for the integral gains.

5.3. Startup Under Varying Load

The most challenging part of BLDC motor control is to determine the proper commutation sequence and timing during the startup stage where there is no BEMF signal available to determine the rotor position. If the motor load is known, then the step durations can be calibrated for a specific acceleration rate and these step durations can be used during blind commutation. On the other hand, if the motor load varies from one startup to another, then it will not be possible to rely on any calibration data. The driver algorithm should dynamically change the drive parameters as the rotor accelerates at an unknown rate. There are two critical requirements of this process:

1. Determine the actual acceleration rate and calculate the required commutation step durations.
2. Maintain the rotor position at the required rotation angles for each commutation step so that the optimum torque angle can be obtained in the following steps.

The experiments to test the startup algorithm with variable load conditions were carried out by using six different inertial loads that are listed as M1 through M6 in Table 5.3. The inertial loads were obtained by installing different number of steel washers on a rod mounted on the rotor as shown in Figure 5.17. The motor used in this experiment was 57BL55S06 that can provide maximum of 0.18 Nm torque at 3.3 A rated current. The commutation step durations that had been previously determined for the lowest load M1 were set as the initial step durations at the beginning of the startup. The startup algorithm detected rotor position by using inductive sense method after the first step and calculated the next step duration according to the estimated actual rotor acceleration. The same sequence of position detection, estimation of acceleration, and step calculation was repeated until the end of the sixth step.

Table 5.3. Rotational inertia of loads.

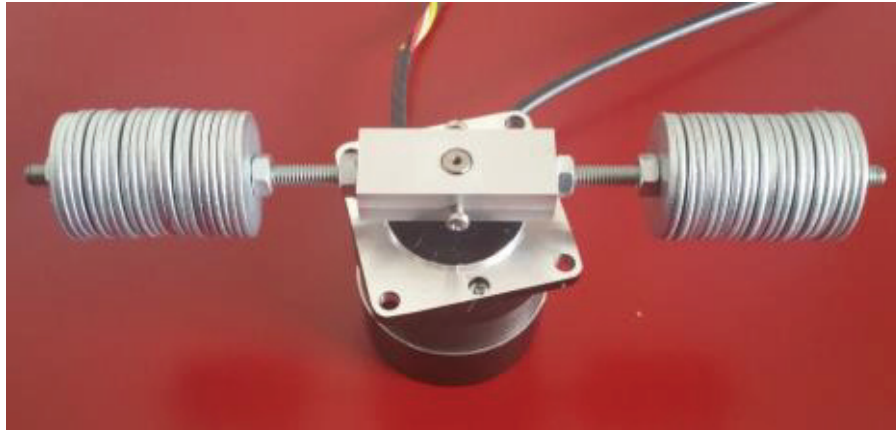| M1	0.000542 kg.m^2
M2	0.001126 kg.m^2
M3	0.001635 kg.m^2
M4	0.002202 kg.m^2
M5	0.002746 kg.m^2
M6	0.003272 kg.m^2

Figure 5.17. Mechanism of variable load test.

Performance of the startup algorithm was evaluated by comparing the step durations calculated by the algorithm with the step durations that are expected as a result of the ratio of the inertial loads. A complete list of commutation step durations is given in Table 5.4 and the same results are also shown graphically in Figure 5.18.

Table 5.4. Commutation step durations calculated by the startup algorithm depending on the varying inertial loads given by M1 through M6.

| TX(µs)	1	2	3	4	5	6	7	8	9	10	11	12
M1	100000	44596	36176	26312	26204	23980	22312	21004	19944	19060	18308	17656
M2	100000	52400	44400	38576	40024	35476	32312	29944	28088	26580	25324	24256
M3	100000	63760	55356	42492	39196	42388	38092	34976	32588	30676	29108	27784
M4	100000	93648	58176	49872	44052	48708	43552	39848	37028	34780	32940	31396
M5	100000	71496	88668	68356	56144	50096	45764	42464	39840	37688	35884	34344
M6	100000	80276	84836	61608	57192	56336	50260	45908	42596	39960	37804	35992
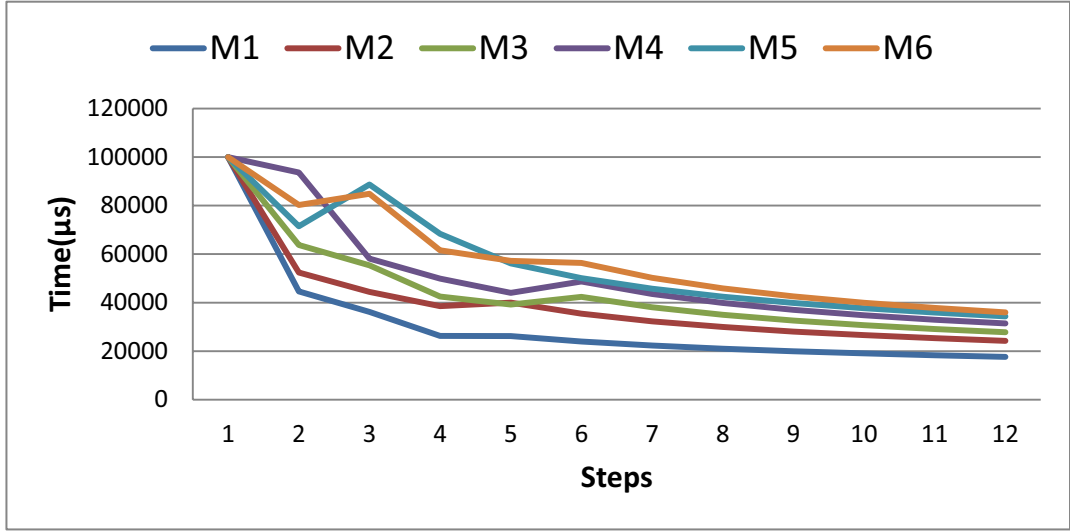
Figure 5.18. Step durations for varying load.

Looking at the results of the algorithm, the time increases as the load increases as expected. When M2 and M1 are compared, the ratio expected between the corresponding commutation step durations is given by

$$T_{\text{M2}}(k) = \sqrt{\frac{M2}{M1}}\, T_{\text{M1}}(k) \tag{5.1}$$

since this ratio is proportional to the square root of the load. When it is examined for the 6'th step time:

$$T_{\text{M2}}(6) = \sqrt{\frac{0.001126\ \text{kg.}\,\text{m}^2}{0.000542\ \text{kg.}\,\text{m}^2}}\, 23980\ \mu\text{s} \tag{5.2}$$

estimated time for M2 at 6'th step is

$$T_{\text{M2}}(6) = 34564\mu\text{s} \tag{5.3}$$

whereas the experimentally obtained time for M2 at 6'th step is 35436 µs.
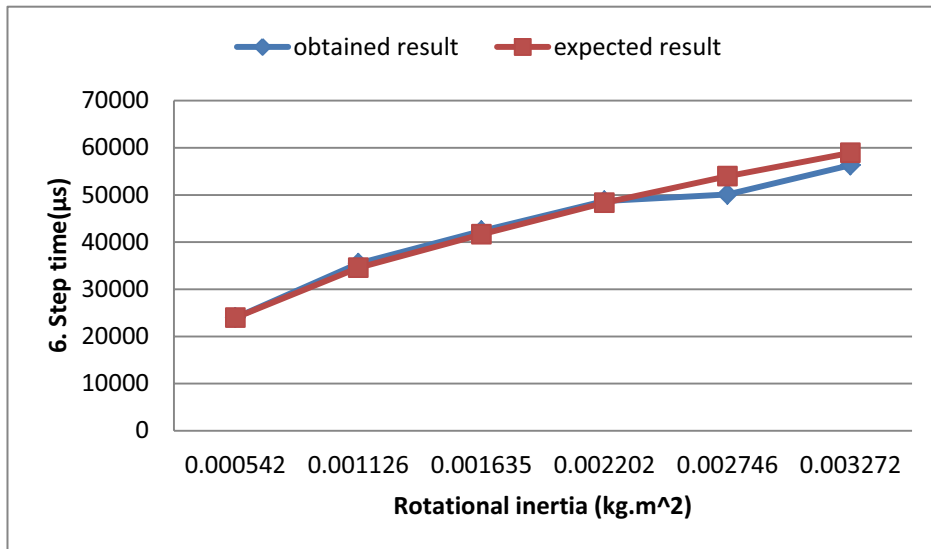
Figure 5.19. Sixth step time versus rotational inertia.

The load estimation is made depending on the changes in the motor load by taking advantage of the position finding by using the inductive sense method. The step duration was determined according to the load, using the acceleration change. The sixth obtained step time was shown in Figure 5.19. In addition, the algorithm provided rotor with exact step zone alignment to produce maximum torque as shown in Figure 5.20.

Figure 5.20. Step alignment.

CHAPTER 6

CONCLUSION

Three new methods for brushless DC motor control were successfully implemented for varying load conditions in this thesis. First, a simple empirical for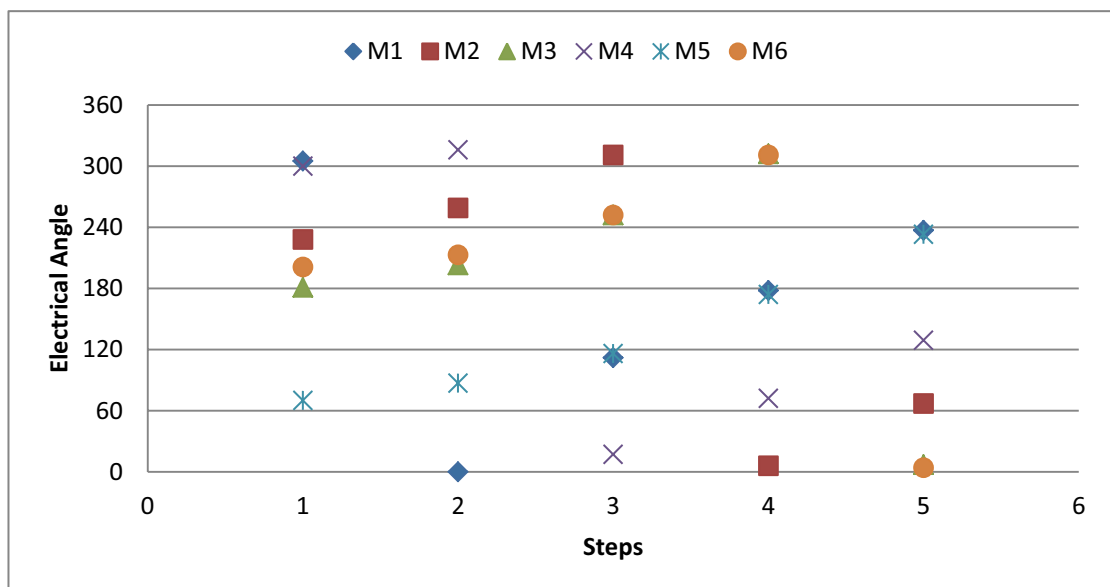mula was used for accurate position detection based on the inductive sense method. Afterwards, the precise position information was utilized to estimate the motor load in a start-up algorithm for on the run calculation of commutation step durations during acceleration. The third improvement was the implementation of a dynamically sized BEMF zero-cross detection window that allowed fast controller response to abrupt speed changes during synchronous commutation with speed regulation. Optimized coding techniques were used to implement these methods on an eight-bit microcontroller.

The sensorless methods for position detection involve rather complex algorithms, but they provide more economical and physically less complex solutions. Inductive sense method was used to improve the startup algorithm under variable load conditions, since BEMF detection is useless at stand still and low speed. Then, the position information was used to determine driver parameters during startup acceleration. The driver dynamically controlled commutation step durations during startup depending on the load on the motor. The control algorithm estimated the output load according to the actual acceleration rate that can be found accurately based on the precise rotor position detected by using the inductive sense method. The start up algorithm also calculated the required rotation angle for each commutation step to maintain the optimum torque angle and the best possible power efficiency during start up process.

The proposed startup method was verified by using six different inertial loads on a brushless DC motor. The performance analysis was made by comparing the step durations calculated by the startup algorithm with the expected step durations calculated according to the inertial load values. The results were compared with the required step durations for each inertial load setting, and it was observed that, the results are proportional to the square root of the inertial loads as expected.

In the future work, the position calculation based on inductance variation of stator windings can be done by using only three excitation steps instead of measuring rise times for all six steps. Once the initial rotor position is determined, the expected rotor position after each commutation step can easily be estimated, and the three excitation steps required for precise position calculation can be chosen around the estimated position. The total time spent in inductive sense can be reduced and a higher acceleration rate can be obtained during startup.

Another future application is the adaptation of startup algorithm for periodic load variations where the torque requirement varies as a function of the mechanical angle. If the torque variation can be determined during the first mechanical revolution, then proper arrangement of the commutation steps in the following revolutions can be possible.

REFERENCES

Aiguo, ZHOU, YANG Lang, and PAN Qiangbiao. 2015. 'Rotor Position Detection and Start-up Methods of a Sensorless BLDC Motor'. 2015 IEEE Advanced Information Technology, Electronic and Automation Control Conference (IAEAC), 1092–96.

Atmel AVR498. 2009. 'Sensorless Control of BLDC Motors Using ATtiny261/461/861'. Atmel AVR498 Application Note. Accessed November 28, 2016. http://ww1.microchip.com/downloads/en/appnotes/doc8192.pdf.

Atmel AVR928. 2013. 'Scalar Sensorless Methods to Drive BLDC Motors'. Atmel AVR928 Application Note. Accessed December 22, 2016. http://ww1.microchip.com/downloads/en/appnotes/atmel-8305-avr928-scalar-sensorless-methods-to-drive-bldc-motors_application-note.pdf.

Bado, A., S. Bolognani, and M. Zigliotto. 1992. 'Effective Estimation of Speed and Rotor Position of a Pm Synchronous Motor Drive By a Kalman Filtering Technique'. Power Electronics Specialists Conference, 1992. PESC '92 Record., 23rd Annual IEEE 2: 951–57.

Chang, Yen-Chuan, and Ying-Yu Tzou. 2007. 'A New Sensorless Starting Method for Brushless DC Motors without Reversing Rotation'. PESC Record - IEEE Annual Power Electronics Specialists Conference, 619–25. doi:10.1109/PESC.2007.4342058.

Consoli, Alfio, Salvatore Musumeci, Angelo Raciti, and Antonio Testa. 1994. 'Sensorless Vector and Speed Control of Brushless Motor Drives'. IEEE Transactions on Industrial Electronics 41 (1): 91–96.

Dhaouadi, R., N. Mohan, and L. Norum. 1991. 'Design and Implementation of an Extended Kalman Filter for the State Estimation of a Permanent Magnet Synchronous Motor'. IEEE Transactions on Power Electronics 6 (3): 491–97. doi:10.1109/63.85891.

Gamazo-Real, José Carlos, Ernesto Vázquez-Sánchez, and Jaime Gómez-Gil. 2010. 'Position and Speed Control of Brushless Dc Motors Using Sensorless Techniques and Application Trends'. Sensors 10 (7): 6901–47. doi:10.3390/s100706901.

Hall, E. H. 1879. 'On a New Action of the Magnet on Electric Currents'. American Journal of Mathematics 2 (3): 287–92.

Hanselman, Duane. 2006. Brushless Permanent Magnet Motor Design. MAGNA

PHYSICS PUBLISHING.

Harris Semiconductor. 1996. '80V, 0.5A Three Phase Driver'. HARRIS Corporation Datasheet HIP4086. Accessed January 23, 2016. http://www.farnell.com/datasheets/30883.pdf.

Hoque, M.A., and M.A. Rahman. 1994. 'Speed and Position Sensorless Permanent Magnet Synchronous Motor Drives'. 1994 Proceedings of Canadian Conference on Electrical and Computer Engineering 2 (1): 689–92.

Iizuka, Kenichi, Hideo Uzuhashi, Minoru Kano, Tsunehiro Endo, and Katsuo Mohri. 1985. 'Microcomputer Control for Sensorless Brushless Motor'. IEEE Transactions on Industry Applications IA-21 (4): 595–601. doi:10.1109/TIA.1985.349715.

Ikhlas, Muhammad. 2015. 'Rotor Position Identification for Brushless DC Motor'. Master of Engineering Science. The University of Western Ontorio.

Jang, G. H., J. H. Park, and J. H. Chang. 2002. 'Position Detection and Start-up Algorithm of a Rotor in a Sensorless BLDC Motor Utilising Inductance Variation'. IEE Proceedings - Electric Power Applications 149 (2): 137–42. doi:10.1049/ip-epa:20020022.

Johnson, James P., M. Ehsani, and Yılcan Guzelgunler. 1999. 'Review of Sensorless Methods for Brushless DC'. Conference Record of the 1999 IEEE Industry Applications Conference. Thirty-Forth IAS Annual Meeting 1: 143–50. doi:10.1109/IAS.1999.799944.

Lai, Yen Shin, Fu S. Shyu, and Shian Shau Tseng. 2003. 'New Initial Position Detection Technique for Three-Phase Brushless DC Motor without Position and Current Sensors'. IEEE Transactions on Industry Applications 39 (2): 485–91. doi:10.1109/TIA.2003.809450.

Lita, Adrian, and Mihai Cheles. 2008. 'Sensorless BLDC Control with Back-EMF Filtering Using a Majority Function'. Micrchip Corp. Application Note AN1160, 1–24.

Liu, Tian-Hua, and Chien-Ping Cheng. 1992. 'Adaptive Control for a Sensorless Permanent-Magnet Synchronous Motor Drive'. Proceedings of the 1992 International Conference on Industrial Electronics, Control, Instrumentation, and Automation 1 (3): 413–18.

Matsui, Nobuyuki, and Masakane Shigyo. 1990. 'Brushless DC Motor Control without Position and Speed Sensors'. IEEE Conferences 1: 448–53.

Miller, T. J. E. 1989. Brushless Permanent-Magnet and Reluctance Motor Drives. OXFORD SCIENCE PUBLICATIONS.

Mingyao, Lin, Zhang Zhiyao, and Lin Keman. 2008. 'A Novel and Easy-Realizing Initial Rotor Position Detection Method and Speedup Algorithm for Sensorless BLDC Motor Drives'. 2008 International Conference on Electrical Machines and Systems, 2860–65.

Moreira, Julio C. 1996. 'Indirect Sensing for Rotor Flux Position of Permanent Magnet AC Motors Operating Over a Wide Speed Range'. IEEE Transactions on Industry Applications 32 (6): 1394–1401. doi:10.1109/28.556643.

Nilsson, Christoffer, and Daniel Modrack. 2013. 'Universal Embedded Motor Control'. Master's Thesis in Embedded Electronic System Design. Chalmers University of Technology.

Ogarawara, Satoshi, and Hirofumi Akagi. 1991. 'An Approach to Position Sensorless Drive for Brushless DC Motors'. IEEE Transactions on Lndustry Applicalions 3 (27): 443–47.

Polka, Dave. 2003. Motors and Drives. ISA-The Instrumentation, Systems, and Automation Society.

STMicroelectronics. 2000. 'BLDC Motor Start Routine for the ST72141 Microcontroller'. AN1276 Application Note. Accessed January 22, 2017. https://forums.parallax.com/uploads/attachments/44920/82579.pdf.

Texas Instruments. 2017. 'DRV10983x, DRV10975x, and DRV10987 IPD Tuning Guide'. Texas Instruments User's Guide SLOU426. Accessed November 1, 2017. http://www.ti.com/lit/ug/slou426a/slou426a.pdf.

Wu, Rusong, and Gordon R. Slemon. 1990. 'A Permanent Magnet Motor Drive without a Shaft Sensor'. Conference Record of the 1990 IEEE Industry Applications Society Annual Meeting 27 (5): 553–58. doi:10.1109/IAS.1990.152239.

Yedamale, Padmaraja. 2003. 'Brushless DC (BLDC) Motor Fundamentals'. Microchip Technology Inc., 1–20.